Superdeformed bands in $^{80-83}$Sr, $^{82-84}$Y, ^{83,84}Zr: Transition quadrupole moments, moments of inertia, and configuration assignments

F. Lerma,* W. Reviol,† C. J. Chiara, M. Devlin,‡ D. R. LaFosse, and D. G. Sarantites
Department of Chemistry, Washington University, St. Louis, Missouri 63130

C. Baktash and H.-Q. Jin§
Physics Division, Oak Ridge National Laboratory, Oak Ridge, Tennessee 37830

R. M. Clark, I. Y. Lee, and A. O. Macchiavelli
Nuclear Science Division, Lawrence Berkeley National Laboratory, Berkeley, California 94720

W. Satuła
Institute of Theoretical Physics, Warsaw University, Hoża 69, Warsaw PL-00681, Poland

D. Soltysik and S. L. Tabor
Department of Physics, Florida State University, Tallahassee, Florida 32306

R. Wyss
KTH, Department of Physics-Frescati, Frescativägen 24, Stockholm S-104 05, Sweden
(Received 5 February 2002; published 28 April 2003)

Multiple superdeformed bands in the nuclei $^{80-83}$Sr, $^{82-84}$Y, and ^{83,84}Zr have been studied in a backed-target experiment, using the Gammasphere and the Microball 4π detector arrays. For 15 bands in these nuclei, average transition quadrupole moments have been measured with high accuracy, using the Doppler-shift attenuation method. Among these are the newly observed superdeformed bands in ^{83,84}Y, which are ''isospectral'' with the bands in ^{82,83} Sr. These ''isospectral'' bands have nearly identical transition quadrupole moments. Two of the bands in ^{81}Sr interact and cross transitions between them are observed. The present measurements place stringent conditions on configuration assignments for the bands obtained from two types of mean-field calculations, leading to a consistent understanding of the mass ~80 superdeformed bands. The assignments for different bands arise from one or more nucleons occupying the $N_0=5h_{11/2}$ intruder orbital.

DOI: 10.1103/PhysRevC.67.044310 PACS number(s): 27.60.+j, 23.20.Lv, 21.60.Cs

I. INTRODUCTION

The search for superdeformed (SD) bands in the nuclear region around mass 80 was initiated by predictions for very elongated shapes with a major-to-minor axis ratio of 2:1 in nuclei with atomic number $Z=38-40$ and neutron number $N=42-45$ [1–6]. Eight years ago, these predictions were experimentally confirmed with the observation of a SD band in ^{83}Sr [7,8]. Since then, significant improvements in the detection capabilities have allowed one to unravel an island of SD shapes at high spin in this nuclear region. To date, SD bands have been found in $^{80-83}$Sr [7–12], $^{82-84}$Y [13,14], ^{83,84,86}Zr [15–17], ^{85,87}Nb [18,19], ^{88}Mo [20], and ^{89,91}Tc [21,22]. These bands are observed up to a rotational frequency of about 1.3 MeV/$\hbar$, a value twice as high as the maximum frequencies encountered for the SD bands in the next heavier region of SD shapes around mass 150. Therefore, the study of the properties of these SD bands remains a challenging task.

The SD nuclei in the mass-80 region are theoretically described as prolate deformed rotors with a quadrupole deformation of $\beta_2\sim 0.5$. This picture is supported by the large dynamic moments of inertia $\mathcal{J}^{(2)}$, obtained for the SD bands in the mass-80 region, which have on average a value of $\sim 25\,\hbar^2/\mathrm{MeV}$.[1] In some cases, the deformations of these bands could be directly confirmed by measuring their average transition quadrupole moments Q_t, with the residual Doppler-shift method [23]. These lifetime measurements, all prior to the present work, are reported in Refs. [9,11,15–17].

The deformation and thus the Q_t value depends sensitively on the number of high-j intruder orbitals involved in the formation of the SD shape. In the mass-80 region, the intruder orbitals that are located at the SD shell gaps are those with $N_0=5h_{11/2}$ parentage. The Q_t value measured for a particular SD band ought to be characteristic for the intruder content of its underlying configuration. This allows

*Present address: Radiation Oncology Center, Washington University, St. Louis, MO 63110.
†Corresponding author. Electronic address: reviol@wuchem.wustl.edu
‡Present address: LANSCE-3, MS H855, LANL, Los Alamos, NM 87545.
§Present address: NASA Ames Research Laboratory, MST27A-1, Moffett Field, CA 94035.

[1]The only exception being the SD band in ^{91}Tc, the heaviest nucleus under consideration, which exhibits a $\mathcal{J}^{(2)}$ moment between 35 and 40 $\hbar^2$/MeV.

one to obtain a reliable configuration assignment similar to those for the SD nuclei in the mass-150 region. Interestingly, a SD shell gap is predicted to develop at particle number 40 for high rotational frequency but is absent at $\hbar\omega=0$. This complicates matters for the proton system. In contrast, the SD gap at particle number 44 that is most relevant for the neutron system is found to be very pronounced over the whole frequency range observed.

While the results of the previous Q_t measurements helped to establish the SD shape, they were somewhat unsatisfying for two reasons. Of concern were the large experimental uncertainties (relative errors between 15% and 40%) of the Q_t values. This did not allow testing of the theoretically predicted trends for the SD shapes as a function of Z and N throughout the mass region and made configuration assignments rather difficult. A second shortfall was the lack of lifetime information for the yrast SD bands in some isotopic chains, e.g., the yttrium isotopes, and the absence of such information for any excited SD band in the mass-80 region. This situation called for new Q_t measurements.

In this paper, we present a comprehensive study of SD bands in nine different nuclei in the mass-80 region, viz., in $^{80-83}$Sr, $^{82-84}$Y, and ^{83,84}Zr. In most of these nuclei, multiple SD bands are observed. Among the 21 SD bands reported seven bands are newly observed or reported in detail for the first time. The most important results are the accurately measured Q_t values of 15 of these bands. These values are obtained by using the residual Doppler-shift method. However, unlike in previous experiments the measurements have been performed with a single target with backing. From the trends for the experimental Q_t values and $\mathcal{J}^{(2)}$ moments as a function of Z and N, configuration assignments for $Z=38-40$ and $N=42-45$ SD nuclei are proposed and some of the previously made assignments are revised. Four of these SD bands are viewed as pairs of ''spectrally identical'' or isospectral bands and their properties are studied in detail based on their measured Q_t values. The Q_t measurements for six yrast SD bands observed in the present data have been reported in a Letter [24]. Here, additional results, which include several excited SD bands, as well as more details than in Ref. [24] are presented.

II. EXPERIMENTAL DETAILS

In order to avoid the limitations of previous experiments in accurately measuring Q_t values for the SD bands in the mass-80 region, care was taken to maximize the sensitivity to the lifetimes of those bands and reduce variations in the systematic errors of the extracted lifetime values. A single 570 μg/cm^2 ^{58}Ni target foil backed with 3.2 mg/cm^2 of gold was employed in two separate reactions. In the first reaction, the target was bombarded with a ^{28}Si beam at 130 MeV, populating high spin states in ^{80,82}Sr, ^{82,83}Y, and ^{83}Zr via $\alpha 2p$, $4p$, $3pn$, $3p$, and $2pn$ fusion-evaporation exit channels, respectively. In the second reaction, a ^{29}Si beam at 130 MeV was used to populate high-spin states in ^{81,83}Sr, ^{84}Y, and ^{84}Zr via $\alpha 2p$, $4p$, $3p$, and $2pn$ exit channels, respectively.

The experiment was performed at the 88-Inch Cyclotron at the Lawrence Berkeley National Laboratory. The γ rays emitted from the reactions were detected with the Gammasphere array [25], which consisted of 100 hyperpure Ge detectors fitted with bismuth germanate (BGO) shields to obtain Compton-suppressed γ-ray spectra. The Gammasphere detectors are arranged in 17 angular rings. The emitted charged particles were detected with a Microball, a 95-element CsI(Tl) 4π detector array [26]. The Microball served a twofold purpose. First, its high efficiency and good charged particle identification capability based on a pulse-shape discrimination technique were used for selecting the exit channels of interest in the subsequent analysis. Second, the reasonably good energy resolution of the Microball allowed reconstruction of the momenta of the recoiling nuclei. This permitted a precise Doppler shift correction of the γ-ray energies. To optimize the selectivity for the exit channels, the hevimet collimators of Gammasphere were removed during the experiment and total γ-ray pulse height H_γ, and γ-ray fold k_γ, information were measured for each event [27].

The event trigger required a minimum of four Compton-suppressed γ rays in prompt coincidence. Any pulse height and time information from the Microball that was correlated with the event trigger was accepted as well. Two days of running time were spent for each reaction and $\sim 9\times 10^8$ events per run were collected.

III. ANALYSIS

Using the charged particle identification provided by the Microball, the data were sorted according to individual exit channels. Residual contaminants in the particle gates resulting from unidentified protons, α particles, and neutrons were sharply reduced by placing correlated gates on (H_γ, E^*), the total γ-ray pulse height, H_γ, and excitation energy, E^*. Here, E^* was obtained from the relation $E^*=T_{\text{c.m.}}-\Sigma(E_{particle})$, where $T_{\text{c.m.}}$ is the kinetic energy of the collision in the center of mass system [28].

The γ-ray energy spectra display Doppler shifts, which decrease as a function of slowing of the nuclei in the target and backing and become constant when they escape from the backing. In order to correct the Doppler shifts and sharpen the E_γ spectra, the energies of the detected charged particles were used to reconstruct the momenta and, consequently, the initial recoil velocity of the recoiling nuclei on an event-by-event basis. To take into account the slowing of the recoils, a γ-ray energy dependent recoil velocity β_{app} was introduced and this function was optimized for SD transitions of interest. This procedure led to an accurate Doppler-shift correction for the inband SD transitions (and to broader peaks for the slower transitions).

The resultant Doppler-shift corrected parameters E_γ of coincident γ-ray transitions in individual exit channels were sorted into two sets of histograms. First, a symmetrized $E_\gamma - E_\gamma$ matrix and an $E_\gamma - E_\gamma - E_\gamma$ cube for the Gammasphere detectors at all detector angles were created. These two- and three-dimensional histograms were used to search for new SD bands and reanalyze previously reported SD bands. Second, the data were sorted into a set of seven $E_\gamma - E_\gamma$ matrices according to angular segments of the Gammasphere array.

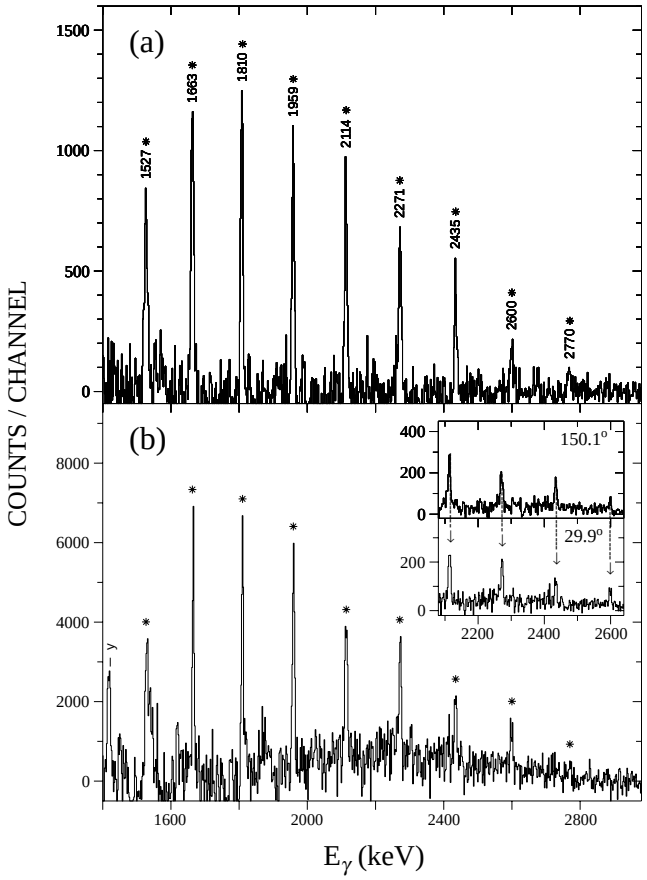

FIG. 1. Sample γ-ray spectra for the SD band in ^{84}Zr, resulting from (a) a double-gating procedure applied to the coincidence cube and (b) sums of gates placed on the coincidence matrix. The gating transitions are marked by an asterisk and a known yrast transition in the nucleus is indicated by ''y.'' The inserts in panel (b) contain spectra gated by several SD transitions for two groups of detectors at average angles of 29.9° and 150.1° with respect to the beam axis.

The *x* axis of these matrices represented only the events from the detectors in a certain angular segment, while the *y* axis included those from any other detector. The angular segments represented groups of detector rings in the array, namely, with average angles $\overline{\theta}$=29.9°, 52.9°, 74.3°, 90.0°, 105.1°, 127.1°, and 150.1° which are symmetric with respect to the 90.0° position. The angle-sorted matrices were prepared to measure the residual shifts of the centroids of the SD band members.

Subsequently, gates were placed on the energies of clean transitions in the SD bands, and one-dimensional spectra were projected out from the matrices and cubes. In the case of the angle-sorted matrices, the projection contained the counts measured in the angular segment $\overline{\theta}$. As an example, spectra for the SD band in ^{84}Zr are shown in Fig. 1. Displayed in panel (a) is the coincidence spectrum obtained from a sum of double gates on inband transitions applied to the cube. The spectra in panel (b) are created by summing the projections from several clean individual gates on transitions of the SD band. The inserts in this panel show a part of the coincidence spectrum at two opposite angle positions as obtained from the corresponding angle-sorted matrices. The markers indicate the shifts of the peak centroids between the different angles. The energy-dependent Doppler-shift correction that was applied to line up E_γ removed most of the Doppler shift. Consequently, the residual shifts that were determined experimentally were small. Nevertheless, they could be determined precisely by careful analysis.

From the measured centroid shifts for the members of a SD band, a velocity β_{res} and E_γ^0 were extracted by fitting the seven $(E_\gamma, \overline{\theta})$ pairs for each transition in the band with the expression $E_\gamma = E_\gamma^0\sqrt{1-\beta_{res}^2}/(1-\beta_{res}\cos\overline{\theta})$, using a least-squares procedure. The velocity components, β_{app} and β_{res}, obtained from the applied and the residual Doppler shift of an individual transition, respectively, were added relativistically to obtain an average recoil velocity $\langle\beta\rangle$. This velocity is expressed as a fraction of the initial recoil velocity β_0, i.e., as $\langle\beta\rangle/\beta_0$.

IV. RESULTS

In each final nucleus reported in Sec. II, at least one SD band has been observed. The present data contain in total 21 SD bands, which are listed in Table I. The assignment of a SD band to a particular nucleus is consistent with the observation of strong coincidence relationships between the γ-ray

TABLE I. The SD bands observed in the present work. The reaction channel leading to the final nucleus, the intensity of the band expressed as a fraction of the intensity of the ground-state transition in the nucleus, and the estimated spin for the lowest state (reached by the lowest observed transition) are listed. (The energies of these transitions are given in parentheses.) Notice that the reactions with two different beams, ^{28}Si and ^{29}Si, were used.

Structure	Channel	Yield (%)	Estimated spin ($\hbar$)
^{80}Sr SD1 [a]	$\alpha 2p$	1.17	18 (1443)
^{80}Sr SD2 [a]	$\alpha 2p$	0.52	18 (1688)
^{80}Sr SD3 [a]	$\alpha 2p$	0.36	22 (1846)
^{80}Sr SD4 [a]	$\alpha 2p$	0.13	20 (2140)
^{81}Sr SD1 [b]	$\alpha 2p$	1.02	31/2 (1215)
^{81}Sr SD2 [b]	$\alpha 2p$	0.63	33/2 (1646)
^{81}Sr SD3 [b]	$\alpha 2p$	0.40	47/2 (1883)
^{81}Sr SD4 [b]	$\alpha 2p$	0.29	41/2 (1940)
^{82}Sr [a]	$4p$	0.63	18 (1432)
^{83}Sr [b]	$4p$	1.36	41/2 (1306)
^{82}Y [a]	$3pn$	0.93	16 (1454)
^{83}Y SD1 [a]	$3p$	4.20	45/2 (1893)
^{83}Y SD2 [a]	$3p$	2.94	43/2 (1757)
^{83}Y SD3 [a]	$3p$	2.90	43/2 (1738)
^{83}Y SD4 [a]	$3p$	2.73	45/2 (1920)
^{84}Y SD1 [b]	$3p$	3.02	17 (1460)
^{84}Y SD2 [b]	$3p$	2.72	19 (1810)
^{84}Y SD3 [b]	$3p$	0.76	19 (1880)
^{83}Zr SD1 [a]	$2pn$	6.30	27/2 (1380)
^{83}Zr SD2 [a]	$2pn$	2.69	29/2 (1444)
^{84}Zr [b]	$2pn$	6.40	21 (1527)

[a]Beam ^{28}Si.
[b]Beam ^{29}Si.

TABLE II. Table of energies in keV of all discrete transitions in each SD band observed in this work. The typical uncertainties for the measured energies are 1 keV. For a band in ^{80}Sr (band SD2) and in ^{83}Zr (SD1) ''forking'' is observed as indicated. Transitions given in parentheses are less certain. Notice that the band SD2 in ^{81}Sr has been extended by both a transition at the bottom and at the top.

Band	Individual transition energies (keV)
^{80}Sr SD1	1443, 1611, 1775, 1948,
	2118, 2284, 2441, 2595, 2743, 2426
^{80}Sr SD2	1688, 1821, 1950, 2090, 2256, 2364, 2574
^{80}Sr SD3	1846, 2039, 2216, 2391, 2572
^{80}Sr SD4	2140, 2292, 2459, 2621, 2763
^{81}Sr SD1	1215, 1371, 1520, 1680, 1840, 1988, 2140, 2294,
	2441, 2564, 2661, 2747
^{81}Sr SD2	1646, 1774, 1926, 2084, 2240, 2398, 2540, 2697
^{81}Sr SD3	1883, 2035, 2204, 2369, 2535, 2696
^{81}Sr SD4	1940, 2102, 2260, 2409, 2542
^{82}Sr	1432, 1595, 1756, 1920, 2077, 2230, 2383, 2545
^{83}Sr	1306, 1461, 1613, 1762, 1912,
	2060, 2205, 2347, 2491
^{82}Y	1454, 1605, 1774, 1936, 2100, 2264, 2427, 2582
^{83}Y SD1	1893, 2022, 2156, 2298, 2444, 2586, 2722, (2839)
^{83}Y SD2	1757, 1921, 2072, 2224, 2384, 2551, 2720
^{83}Y SD3	1738, 1871, 2038, 2213, 2378, 2535, 2718
^{83}Y SD4	1920, 2062, 2211, 2374, 2531, 2694
^{84}Y SD1	1460, 1608, 1763, 1912, 2059, 2208, 2354, 2506
^{84}Y SD2	1810, 1959, 2111, 2264, 2412, 2562
^{84}Y SD3	1880, 2038, 2197, 2350, 2508, 1380, 1536, 1640,
^{83}Zr SD1	1749, 1909, 2074, 2241, 2410,
	1427, 1555, 2585, (2761)
^{83}Zr SD2	1444, 1616, 1791, 1964, 2132, 2300, 2466, 2624
^{84}Zr	1527, 1663, 1810, 1959, 2114,
	2271, 2435, 2600, 2770

transitions of the band and prominent transitions near the yrast line of the nucleus. No linking transitions between the SD bands and lower-lying states could be observed. The relative intensities of the SD bands are also reported in Table I together with spin estimates, which are based on intensity considerations as described below.

The γ-ray transitions of the SD bands are listed in Table II. It is assumed that *all* transitions listed in this table are stretched electric quadrupole ($E2$) transitions. This assumption is justified by the measured multipolarities for the transitions of several SD bands. In the literature, multipolarity measurements leading to $E2$ assignments have been reported explicitly for the bands in ^{80}Sr [9], and the yrast bands in ^{83}Sr [8] and ^{83}Zr [15]. In the course of this work, the $E2$ character of certain prominent transitions in ^{81}Sr (bands SD1 and SD3) has been verified in a γ-ray directional correlation analysis. Figure 2 shows for each band a sample γ-ray coincidence spectrum resulting from the corresponding gates on the evaporated charged particles and a sum of gates on several inband γ-ray transitions.

The present analysis confirms the previously reported SD bands in $^{80-83}$Sr (ten bands) [9,10], ^{82}Y (one band) [13], and ^{83,84}Zr (three bands) [16,15]. In the case of ^{81}Sr, a band interaction between bands SD1 and SD3 is observed, which is described in more detail hereafter. In addition to the previously known bands, four new SD bands in ^{83}Y and three new SD bands in ^{84}Y are reported. Among the reported SD bands in the nuclei ^{83,84}Y are two bands isospectral with bands in the neighboring nuclei ^{82,83}Sr. This finding is described in Sec. IV B. The intensity patterns of some of the SD bands and the related issue of spin estimates for the bands (cf. fourth column of Table I) are discussed in Sec. IV C. Finally, the results for the lifetime measurements for all SD bands are reported in Sec. IV D.

A. Band interaction in ^{81}Sr

The presence of four SD bands in ^{81}Sr and an interaction between states of the yrast SD band (band SD1) and those of a nearby level structure have been reported in Ref. [10]. A careful analysis of the coincidence relationships of the SD transitions in each band with other γ rays has revealed ''cross-talk'' between the sequences SD1 and SD3. The interband transitions involved have the respective energies of 1533, 1666, 1691, and 1828 keV and their placement is shown in the level scheme of Fig. 3. The transitions for which an accurate directional correlation analysis was possible (including the interband transitions and the 1883-, 2035-, 2204-, and 2369-keV transitions of band SD3) are found to be of $E2$ character.

The γ-ray spectra shown in Fig. 4 document the coincidence relationships between most of the SD transitions involved in the band interaction. These spectra have been generated from sums of double-gated coincidence spectra to improve the sensitivity for the weaker transitions under consideration.

The band interaction can be attributed to an accidental near degeneracy of states between spins (43/2) and (51/2). As a consequence of this observation, the excited band SD3 has the same parity as the yrast SD band, but its parity cannot be determined from the present evidence. Using a simple two-level mixing picture, the interaction strength obtained is on average ~ 6 keV (for the spin range of $4\hbar$). This information is further discussed in Sec. V C.

B. Isospectral SD bands in ^{82,83}Sr and ^{83,84}Y

Two pairs of spectrally very similar SD bands, termed isospectral here, have been observed in the course of this work, confirming a preliminary observation by Jin *et al.* [14]. The first excited SD band in ^{83}Y (SD2) and the SD band in ^{82}Sr form one pair of isospectral bands, and the yrast SD band in ^{84}Y (SD1) and the SD band in ^{83}Sr form a second pair of isospectral SD bands.

As mentioned above, the SD bands in ^{83}Y and ^{82}Sr were populated in the $3p$- and $4p$-exit channels (of the reaction involving the ^{28}Si beam), and the SD bands in ^{84}Y and ^{83}Sr were populated in the $3p$- and $4p$-exit channels (of the reaction involving the ^{29}Si beam), respectively. However, as shown in Fig. 5, the $3p$-gated data of each reaction contain events from other exit channels, including $4p$ events, which

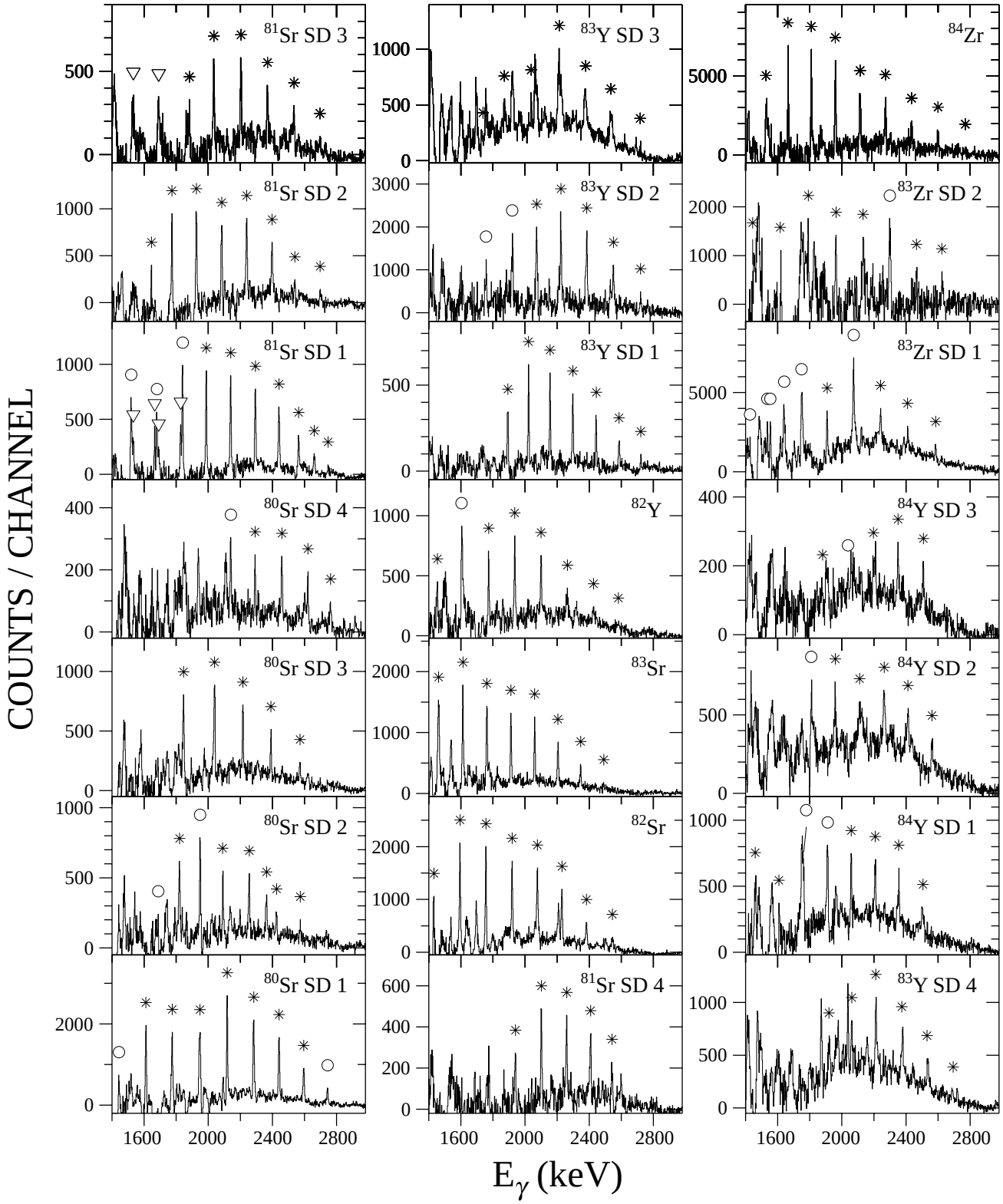

FIG. 2. Sample γ-ray spectra for the SD bands observed in this work. The spectra result from the sums of the gates on in-band transitions, which are indicated by asterisks. The remaining members of each band are indicated by open circles. Two bands in ^{81}Sr interact and the corresponding interband transitions are indicated by triangles. Other prominent γ rays in the spectra, which are not labeled, are either transitions near the yrast line of the nucleus or known contaminant lines. The spectra have a dispersion of 2 keV per channel and the precise γ-ray energies of the SD bands are reported in Table II.

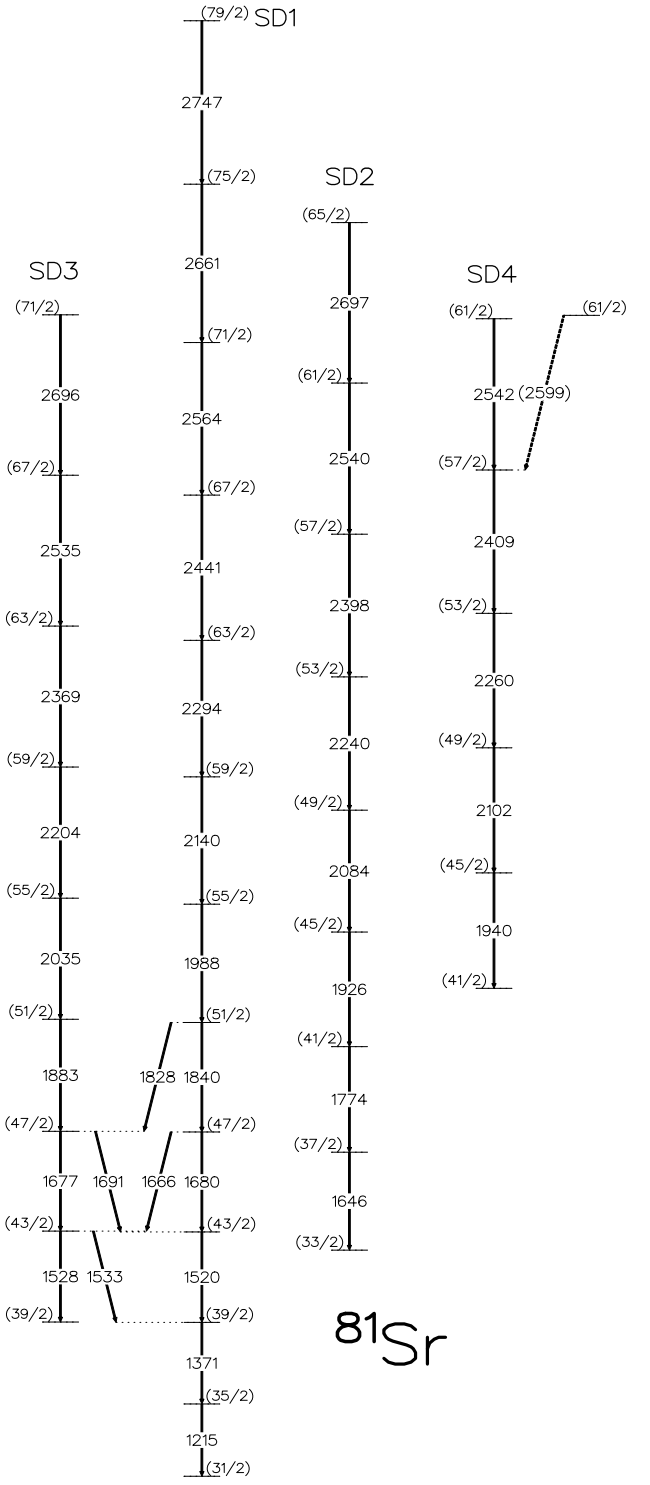

FIG. 3. Level scheme for the SD well in ^{81}Sr. The transitions are labeled by their energies in keV. The spin assignments are based on estimates for the lowest states observed and are therefore tentative.

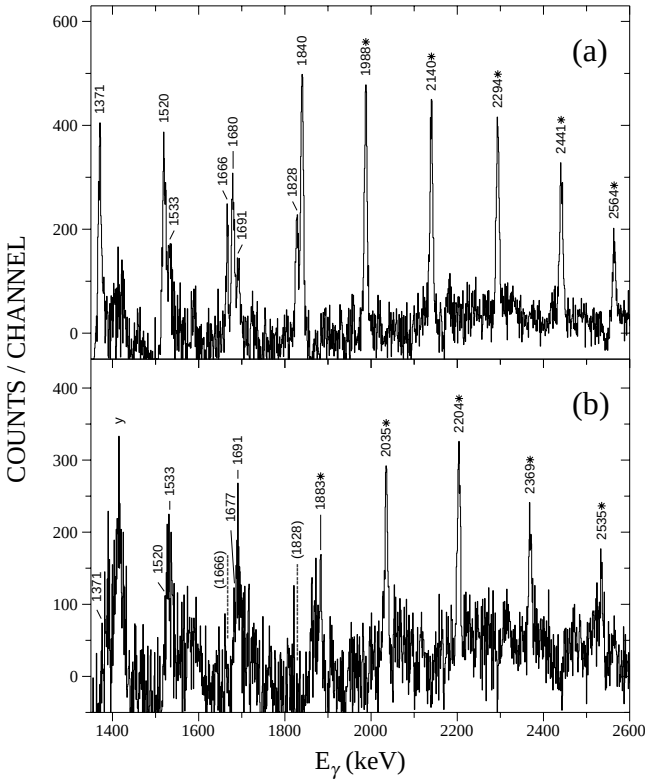

FIG. 4. Coincidence spectra for (a) band SD1 and (b) band SD3 in ^{81}Sr. The asterisks indicate the in-band gating transitions. The remaining transitions are also SD transitions and are placed in the level scheme of Fig. 3. The exception is the γ ray labeled by ''y,'' an yrast transition between normally deformed states.

leak into the $3p$-gated data when only three protons are detected from $4p$ events. Thus, a significant amount of events in which ^{82}Sr and ^{83}Sr were populated leak into the $3p$ data from the ^{28}Si and ^{29}Si reactions, respectively. As a result, the isospectral SD bands in ^{83}Y and ^{84}Y cannot be examined by gating the $3p$ data on their transition γ-ray energies, since their respective isospectral counterparts, in ^{82}Sr and ^{83}Sr, are also observed in these spectra.

In order to isolate the bands in ^{83}Y from the isospectral band in ^{82}Sr and the bands in ^{84}Y from the isospectral band in ^{83}Sr, a complex background subtraction procedure was performed on the $3p$ data from each reaction. The procedure was applied to both sets of $3p$ data in an analogous manner and is, therefore, described in reference to the $3p$ data from the ^{29}Si-induced reaction only.

In the first stage of the background subtraction, the spurious data from various exit channels and low-spin transitions in ^{84}Y present in the $3p$-gated γ-ray spectra were removed by using two-dimensional (H_γ,E^*) gates, as mentioned in Sec. III and described in Ref. [28]. A suitable (H_γ,E^*) gate was found that preferentially selects the ^{84}Y ground band and suppresses the leaking in ^{83}Sr. However, a small amount of ^{83}Sr events remained in this (H_γ, E^*) gated $3p$ data, and were subsequently removed by subtracting a portion of the $4p$-gated events.

The $4p$ data to be subtracted were made to approximate the contaminant ^{83}Sr events, which leak through the (H_γ,E^*) cuts on the $3p$ data. The first step in this procedure was to reproduce the effects of the undetected (fourth) proton in the $3p$ subset. Since the Microball efficiency is lower for low-energy protons (due to threshold effects), the lowest-energy proton of each event was omitted from the evaluation

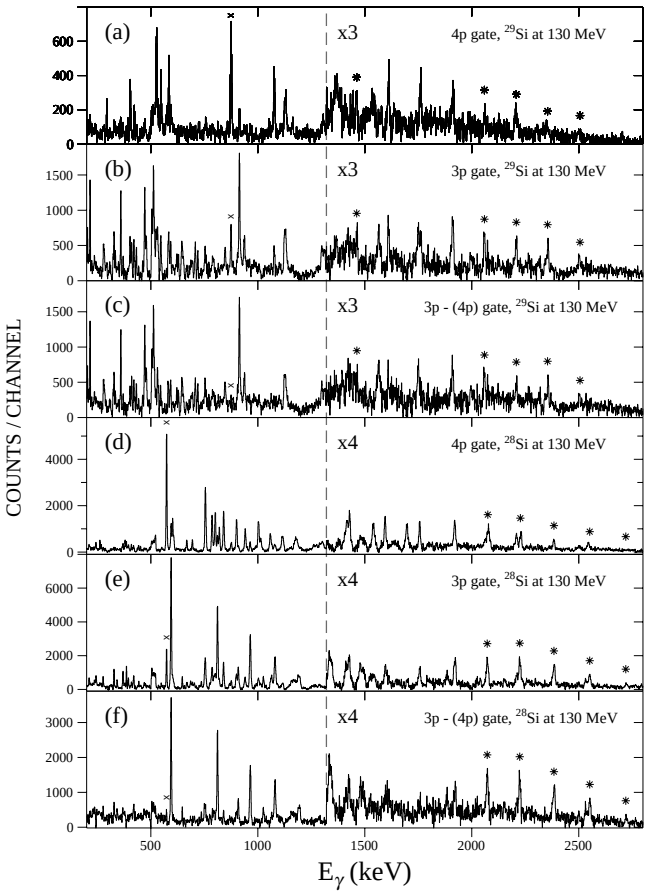

FIG. 5. Panels (a)–(c) contain spectra for the yrast SD band in ^{84}Y, resulting from gates for the in-band γ-ray transitions on the $4p$-gated, $3p$-gated, and $3p$-gated minus $4p$-gated matrices from the ^{29}Si-induced reaction. Panels (d)–(f) contain spectra for the first excited SD band in ^{83}Y, resulting from gates for the in-band transitions on the $4p$-gated, $3p$-gated, and $3p$-gated minus $4p$-gated matrices from the ^{28}Si-induced reaction. The gating γ rays for each matrix are indicated by asterisks. The γ ray marked with an ''x'' in panels (a)–(c) is the strongest transition in ^{83}Sr and the γ ray with the same mark in panels (d)–(f) is the strongest transition in ^{82}Sr. The spectra in panels (c) and (f) demonstrate the removal of the contaminant $4p$ events from the $3p$ gated matrices.

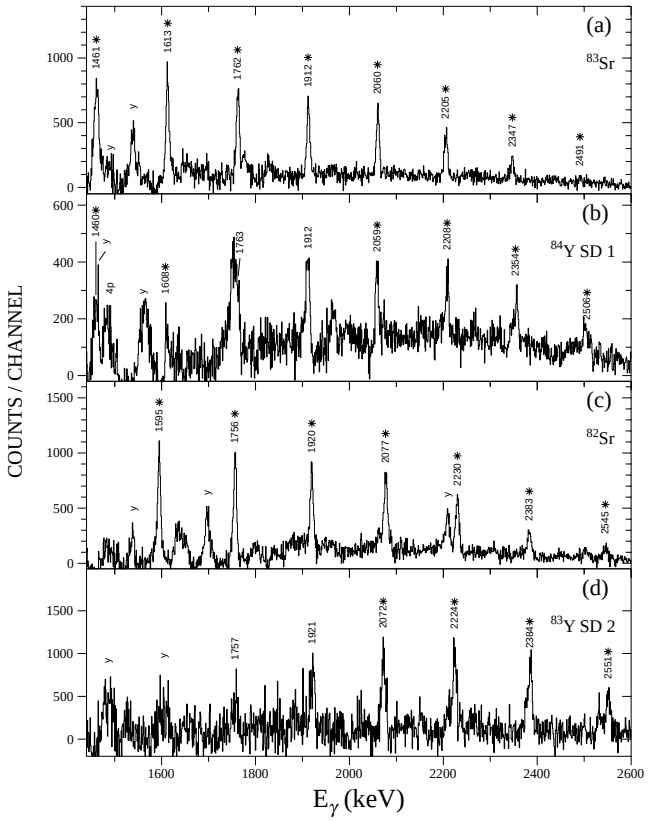

FIG. 6. Portions of the clean spectra of the two pairs of isospectral bands studied in this work. The panels (a) and (b) show the ^{83}Sr-^{84}Y (band SD1) pair, and (c) and (d) show the ^{82}Sr-^{83}Y (band SD2) pair. The transitions are labeled by their energies in keV where the gating transitions are indicated by asterisks. Yrast transtions are labeled by ''y'' and known contaminant transitions by the corresponding reaction channel. The dispersion of the spectra is 1 keV/channel.

of E^* and from the momentum reconstruction employed in the Doppler-shift correction. This procedure is reasonable, since the low-energy protons are most likely missed in the detection of the $4p$ events, and these events thus appear in the $3p$ data. In this way, the E^* profile and the Doppler-shift correction associated with the background $4p$ data approximated well those from the $3p$-gated subset. (Under these conditions, the background $4p$ data produce γ-ray spectra with somewhat reduced resolution compared to those that are obtained when four protons are included in the momentum reconstruction of each $4p$ event.)

The (H_γ,E^*)-cut $3p$ data, and the (H_γ,E^*)-cut $4p$ data, were sorted into $E_\gamma - E_\gamma$ matrices, and an adequate fraction of the $4p$-gated matrix, which was determined from the ratio of the intensities of ^{83}Sr in both datasets, was subtracted from the $3p$-gated matrix to eliminate the remaining ^{83}Sr coincidences in that matrix. The resultant $E_\gamma - E_\gamma$ matrix showed no significant evidence of ^{83}Sr upon gating on the γ-ray energies of decays from that nucleus, and the coincidence of the isospectral SD band with known decays of ^{84}Y was confirmed from the spectra shown in Figs. 5(a)–(c) gated by the transitions of the SD bands.

Following the same procedures, the $3p$ and $4p$ data from the reaction involving the ^{28}Si beam were incremented in an $E_\gamma - E_\gamma$ matrix. In this matrix, the isospectral SD band in ^{83}Y is clearly isolated from the spurious SD band in ^{82}Sr, as seen by the set of its one-dimensional projections shown in Figs. 5(d)–(f).

The spectra for the yrast SD band in ^{84}Y and the excited band SD2 in ^{83}Y after the complex background subtraction are compared in Fig. 6 with the spectra for their respective isospectral bands in ^{83}Sr and ^{82}Sr. For each pair of bands, ^{83}Sr-^{84}Y (a),(b) and ^{82}Sr-^{83}Y (c),(d), the transition energies are strikingly similar over several steps in the γ-ray cascade, i.e., they deviate from each other by at most 5 keV. Consequently, their $\mathcal{J}^{(2)}$ moments are also very similar as discussed below. It is perhaps possible that such a strong similarity could also result from an erroneous background subtraction, in which the $4p$ data were not completely removed from the $3p$ data. However, as stated above, gates on

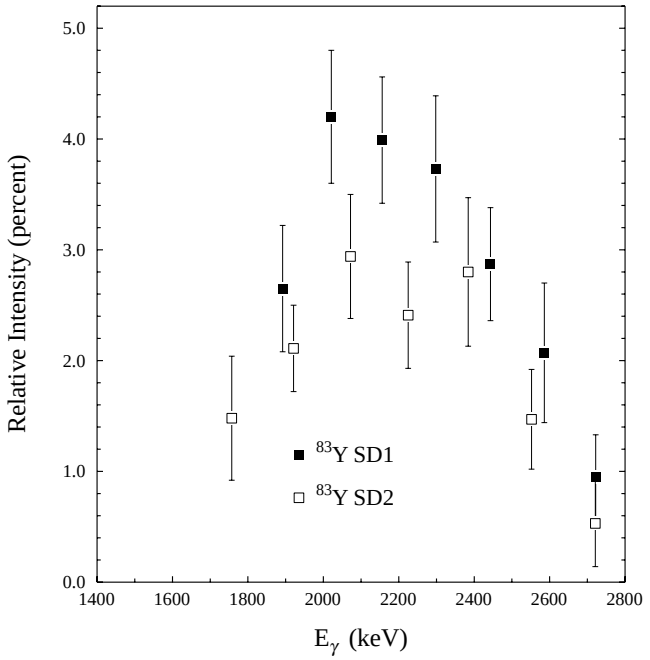

FIG. 7. Relative intensity vs transition energy for two of the newly reported bands in ^{83}Y, SD1 (yrast) and SD2. The intensities of the SD transitions are given relative to the sum of the intensities of the ground-state transitions.

low-lying transitions of the potentially contaminating sequences showed that those contaminants were indeed removed from the $3p$ datasets. Thus, the marginal fraction of the ^{82,83}Sr data, which might remain in the $3p$ data (after the events from the $4p$ channel have been subtracted), cannot account for the presence of the isospectral SD bands in the resultant spectra. The background-subtraction procedures performed establish the existence of the two pairs of SD bands. Therefore, the same procedures were repeated for the centroid shift lifetime analyses for the isospectral bands, and the results are presented in Sec. IV D.

C. Intensities and spin estimates

The relative intensities of the SD bands, obtained from the intensities of the strongest inband γ ray and the ground state transition(s), are reported in Table I. Typical intensity patterns for all members of a particular band are shown in Fig. 7. In the case of the yrast SD band in ^{83}Y, for example, feeding takes place mostly to the top three states in the band, while deexcitation occurs mainly from the bottom two levels.

The coincidence relationships between SD and ''normal'' transitions evaluated for the SD bands reported show that the strength of the decay out is distributed equally among the strongest normally deformed bands.[2] The observed decay features of the bands are consistent with the statistical character of the decays of the SD bands in the heavier mass-150 and mass-190 regions which are known to carry only a few units of angular momentum.

As stated earlier, no linking transitions have been observed. Therefore, spin estimates are made based on the observed feeding into known levels, assuming $2\hbar$ in unseen transitions between the SD and lower spin states. The results of these estimates are reported in Table I (last column).

The spin estimates were checked independently by using a fitting procedure for the measured $\mathcal{J}^{(2)}$ moments of inertia as a function of rotational frequency described in Ref. [29]. For most of the yrast SD bands, a fair agreement is obtained between the estimated spin value of Table I and the result from the fit. The exceptions (no agreement) are those yrast SD bands which extend to rather low transition energies and are subject to irregularities in the E_γ versus spin behavior (bands SD1 of ^{80,81}Sr). Also, poor agreement is obtained for about half of the excited SD bands and this is attributed to the fact that these SD bands are rather short sequences. In conclusion, the spin assignments reported in this paper are reasonable estimates based on the present knowledge.

D. Average Q_t values from lifetime measurements

In order to obtain the average transition quadrupole moments Q_t for the SD bands reported in this paper, the average lifetimes of the SD states were deduced by fitting the calculated fractional Doppler shifts to the measured $\langle\beta\rangle/\beta_0$ values as a function of γ-ray energy for each SD band. This procedure is based on the Doppler-shift attenuation method, where the decay times of the states in the SD band are related to the velocity of the recoiling nuclei as they slow down in the target and backing. Specific for the SD bands under discussion is that several transitions at the top of the band occur already while the recoils traverse the thin target, as known from previous Q_t measurements.

The model calculations for the decay times in the SD band were performed according to a procedure introduced by Lee [30]. In this procedure, the side feeding is modeled based on the measured intensity pattern for the inband transitions, and a constant parameter Q_t is fitted to all levels in the band and those in the side-feeding cascades. Thus, the side feeding times were assumed to be equal to those of preceding inband transitions. The slowing down of the recoils was modeled by using the electronic and nuclear stopping powers provided by the code TRIM [31] and their velocity distribution was calculated as a function of time by integrating over the target and the backing layer. The process of fitting Q_t involves the calculation of the $B(E2)$ value for each transition in the band, using a rotational model with the parameter Q_t, the measured transition energy, and the estimated initial spin of the transition. The best-fit value for Q_t was obtained from a χ^2 minimization with Q_t as a free parameter.

The Q_t values obtained from this modeling may contain systematic uncertainties of the order of 10% from the stopping powers used [31]. For the time scales, and therefore, for the velocities involved in the decay of the SD states, the electronic stopping, which is well known, dominates. This leads to a reduction of the systematic errors due to nuclear

[2]The only exception being the yrast SD band in ^{83}Zr, which decays preferentially to the yrast band.

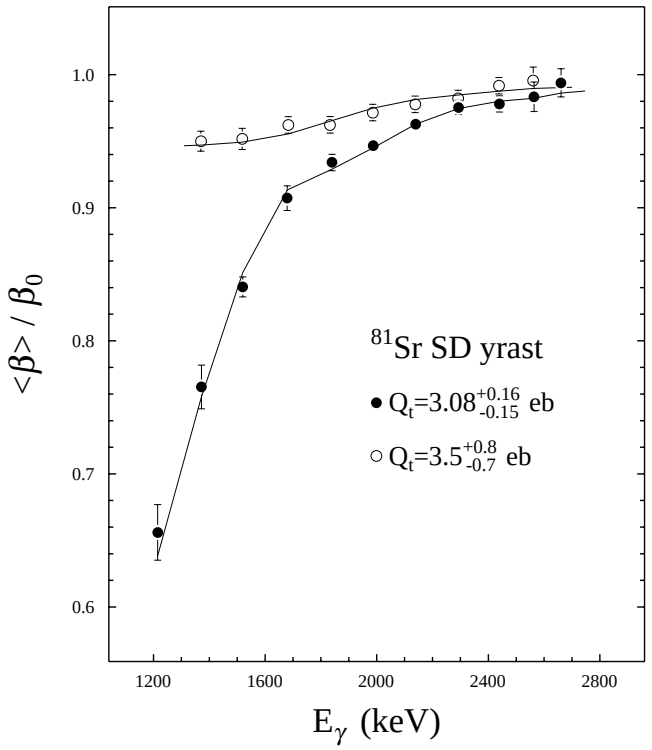

FIG. 8. The fractional Doppler shift for the yrast SD transitions in ^{81}Sr obtained in the present experiment with a backed target (solid circles) compared with the $\langle\beta\rangle/\beta_0$ values for the same SD band in a thin-target experiment [9] (open circles).

stopping in the slowing down process. Furthermore, the uncertainties due to the stopping powers are the same for all measurements in this work and cancel out when the results from the same experiment are compared. Thus, accurate comparisons of Q_t values can be made for evaporation residue nuclei of different Z and N.

The $\langle\beta\rangle/\beta_0$ curves from the present data versus those from previous experiments with a thin target exhibit a significantly increased range in the fractional Doppler shifts. An example for this effect is shown in Fig. 8, where the $\langle\beta\rangle/\beta_0$ values for the yrast SD band in ^{81}Sr from two measurements with different target arrangements are displayed. In the thin-target experiment [9], the conditions under which the ^{81}Sr nucleus was populated were slightly different from the backed-target experiment in that a ^{58}Ni target of thickness 330 μg/cm^2 (not 560 μg/cm^2) was used. The backed target data from the present measurement span a greater reduction in $\langle\beta\rangle/\beta_0$ than those data obtained in the previous experiment [9], in which a thin target was employed. This is due to the additional slowing in the gold backing, during the decay through the middle and the bottom of the SD bands. In the present analysis for the yrast SD band in ^{81}Sr we included the effect of the decay out of the band due to the band interaction (cf. Sec. IV A). This leads to the ''spike'' of the $\langle\beta\rangle/\beta_0$ curve at 1680 keV in Fig. 8 (cf. Fig. 3), and improves the accuracy of the fit to the data.

The datasets, $\langle\beta\rangle/\beta_0$ as a function of E_γ, for the 21 SD bands observed in this work were examined. For most of these bands, Q_t values were determined following the procedure described above. These results are summarized in Table III. Notice that the spins of the band members used for the $\langle\beta\rangle/\beta_0$ fits are based on the estimates discussed earlier (see Table I). The uncertainties they introduce are small compared to other systematic errors that are included in the present results. In Fig. 9, the $\langle\beta\rangle/\beta_0$ curves leading to the Q_t values of Table III are shown. Six out of 21 cases for which no Q_t values are reported suffer from poor statistics due to the weak population of the SD band or/and contaminants introduced by a large background. Therefore, their Q_t values are associated with large errors and are thus meaningless.

TABLE III. Results from the present transition quadrupole moment measurements for SD bands in the mass-80 nuclei and comparison with previous measurements where available. Notice that the present Q_t value for ^{81}Sr SD1 slightly differs from the value reported in Ref. [24]. Notice also that the previous Q_t values for the bands in ^{81,83}Sr as given in Ref. [9] are from reanalyses of the datasets first reported in Refs. [8] and [10], respectively.

Structure	Q_t (e b) present	Q_t (e b) previous	Reference
^{80}Sr SD1	$3.42^{+0.26}_{-0.23}$	$2.7^{+0.7}_{-0.6}$	[9]
^{80}Sr SD2	$3.63^{+0.17}_{-0.15}$	$2.2^{+0.6}_{-0.5}$	[9]
^{80}Sr SD3	4.1 ± 0.6	$3.6^{+2.0}_{-1.1}$	[9]
^{80}Sr SD4	4.9 ± 0.6	$2.8^{+1.1}_{-0.8}$	[9]
^{81}Sr SD1	$3.08^{+0.16}_{-0.15}$	$3.5^{+0.8}_{-0.7}$	[9]
^{81}Sr SD2	$3.30^{+0.27}_{-0.21}$	$3.8^{+0.7}_{-0.5}$	[9]
^{82}Sr	$3.54^{+0.15}_{-0.14}$	$4.5^{+0.9}_{-0.9}$	[11]
^{83}Sr	$3.60^{+0.20}_{-0.18}$	$3.5^{+0.8}_{-0.6}$	[9]
^{82}Y	$4.3^{+1.8}_{-0.8}$		
^{83}Y SD1	4.4 ± 0.7	$4.7^{+0.7}_{-0.7}$	[32]
^{83}Y SD2	$3.6^{+0.8}_{-0.5}$		
^{83}Y SD3	$3.6^{+0.4}_{-0.3}$		
^{84}Y SD1	$3.6^{+0.5}_{-0.9}$		
^{83}Zr SD1	$5.8^{+0.8}_{-0.5}$	$5.0^{+2.0}_{-2.0}$	[15]
^{84}Zr	$5.6^{+0.6}_{-0.5}$	$5.2^{+0.8}_{-0.8}$	[16]

The $^{80-83}$Sr data span the largest ranges in $\langle\beta\rangle/\beta_0$ and, consequently, demonstrate an enhanced sensitivity to the lifetimes of those SD bands. By the same token, the fitted $\langle\beta\rangle/\beta_0$ of the SD bands in $^{82-84}$Y and ^{83,84}Zr indicate reduced ranges in $\langle\beta\rangle/\beta_0$, due to the shorter decay times observed in the yttrium and zirconium cases. Therefore, the Q_t results for $^{80-83}$Sr are obtained with higher accuracy than those for the other cases despite the relatively low yields of the SD bands in the Sr nuclei (cf. Table I).

For a systematic comparison of the isospectral SD bands reported in this paper, the fractional Doppler shifts for the corresponding bands in ^{82}SR, ^{83}Y and ^{83}Sr, ^{84}Y are pairwise shown in Fig. 10. The members of each pair of isospectral SD bands possess very similar Q_t values. In addition to the close resemblance of the sequences of transition energies described earlier, they also have very similar $\mathcal{J}^{(2)}$ moments.

V. DISCUSSION

The main goal of this section is to propose configuration assignments for the SD bands reported. The SD bands in the mass-80 nuclei have been theoretically predicted to arise

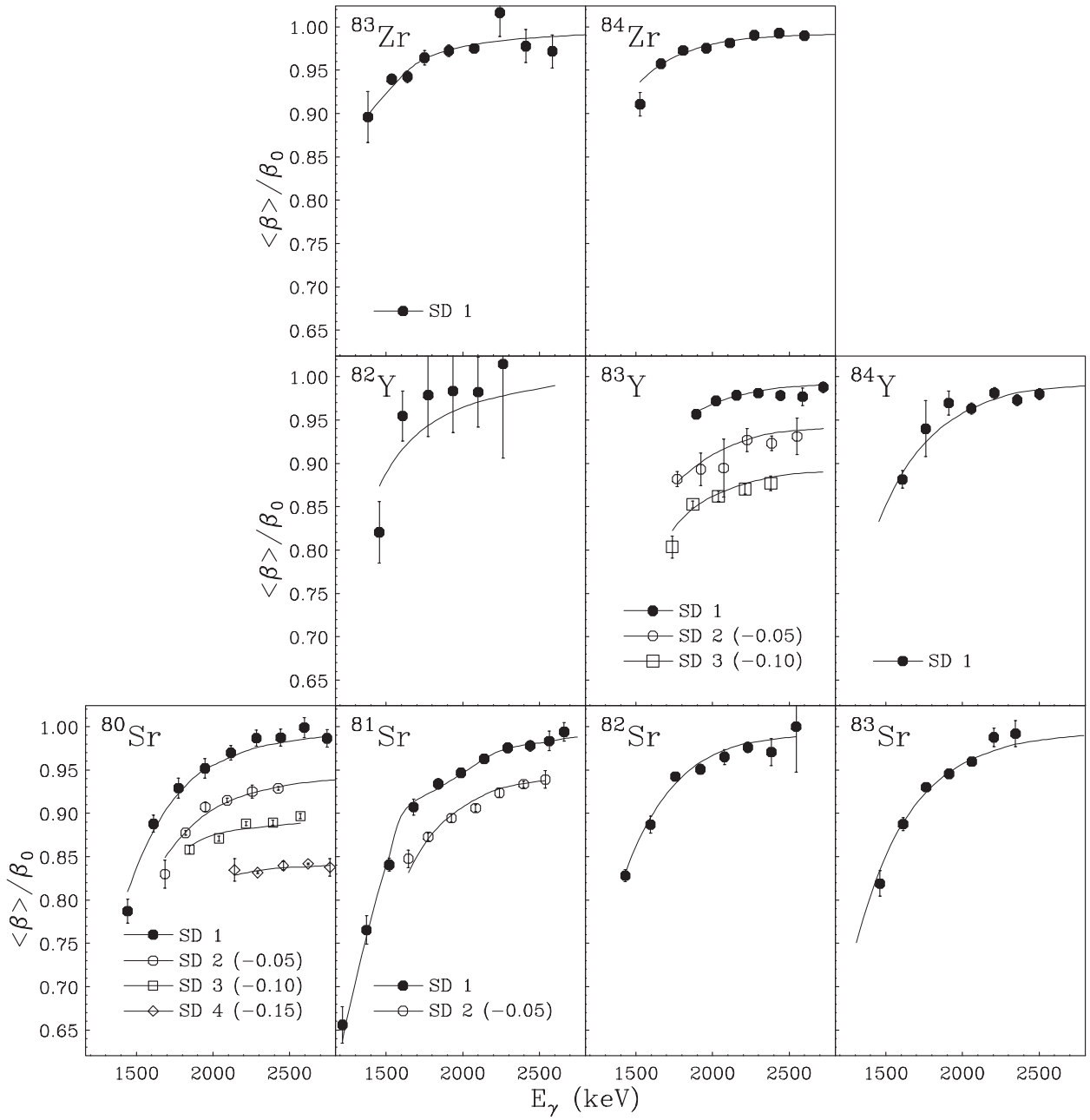

FIG. 9. Fractional Doppler shift $\langle\beta\rangle/\beta_0$ measured for 15 SD bands as a function of γ-ray energy. The $\langle\beta\rangle/\beta_0$ values for the yrast bands are shown as solid circles. The $\langle\beta\rangle/\beta_0$ values for the first, second, and third excited SD bands are reduced by 0.05, 0.10, and 0.15 units and are shown as open circles, open squares, and open diamonds, respectively. The solid lines represent the results from a fitting procedure based on the model calculations decribed in the text.

from the occupation of $h_{11/2}$ intruder orbitals [1,2,4]. Indeed, the configurations assigned to the SD bands observed in this region (see Refs. [7–16]) contain one to four $h_{11/2}$ intruder orbitals, mostly occupied by both neutrons and protons. These configuration assignments were mainly based on comparisons between the calculated and the experimentally observed $\mathcal{J}^{(2)}$ moments of inertia, and only in some cases [9,11,15–17] confirmed by Q_t measurements. However, the latter had large systematic and statistical errors (cf. Table III), and thus did not provide stringent tests for the theoretical calculations. The present results, on the other hand, provide sensitive tests for calculated Q_t values governed by intruder orbital occupations. As a consequence, the configuration assignments presented in Sec. IV C are mainly based on the results from the lifetime measurements.

A. Transition quadrupole moments

1. Trends in Q_t moments of yrast SD bands

The present results for the Q_t moments of the yrast SD bands allow one to establish trends across the mass-80 region. In Fig. 11, the Q_t values of the yrast SD bands in

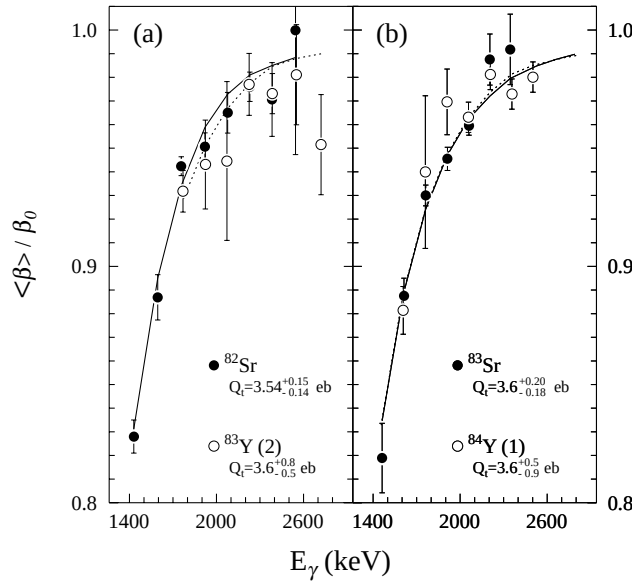

FIG. 10. Comparisons of $\langle\beta\rangle/\beta_0$ vs E_γ data for the pairs of isospectral SD bands reported in this paper. Panel (a) shows the result for the SD band in ^{82}Sr and the first excited SD band in ^{83}Y, panel (b) for the SD band in ^{83}Sr and the yrast SD band in ^{84}Y. The solid and dashed lines correspond to the best fits for Q_t in the Sr and Y isotopes, respectively.

$^{80-83}$Sr, $^{82-84}$Y, and ^{83,84}Zr are plotted as a function of Z and N. The bands in both the $N=43$ and 44 isotones show increasing Q_t values from Sr ($Z=38$) to Zr ($Z=40$). The trend in Q_t as a function of N shows an essentially constant behavior in each isotopic chain under consideration. However, the data are also consistent with moderately decreasing Q_t values for $N\geqslant 44$. Hence, the yrast SD bands in ^{83,84}Zr have the largest values ($Q_t\approx 5.7\ e$ b), while the bands in $^{82-84}$Y ($Q_t\approx 4.3\ e$ b) and $^{80-83}$Sr ($Q_t\approx 3.5\ e$ b) exhibit smaller and rather moderate values, respectively. Clearly, a change of the quadrupole moment depends mainly on Z but not on N. This suggests that the intruder configuration remains unchanged within an isotopic chain, in agreement with the theoretical calculations described below.

2. Q_t moments of excited SD bands

In Fig. 12, the Q_t values of the excited SD bands in ^{80,81}Sr and ^{83}Y are compared with the values for the yrast SD bands in these isotopic chains (the value for the band in ^{83}Sr is omitted for simplicity). Using the average value for the yrast SD bands in the strontium isotopes ($Q_t\approx 3.5\ e$ b, dotted line) as a reference, the following observations can be made. The lowest excited bands in both the strontium and yttrium isotopes have the same Q_t values as the yrast SD bands in $^{80-83}$Sr. This is again suggestive of a very similar intruder configuration for these excited bands. Interestingly, the highest lying band in ^{80}Sr (band SD4) is characterized by a significantly larger Q_t value. This is consistent with the occupation of at least one more intruder orbital as compared to, e.g., the yrast SD configuration.

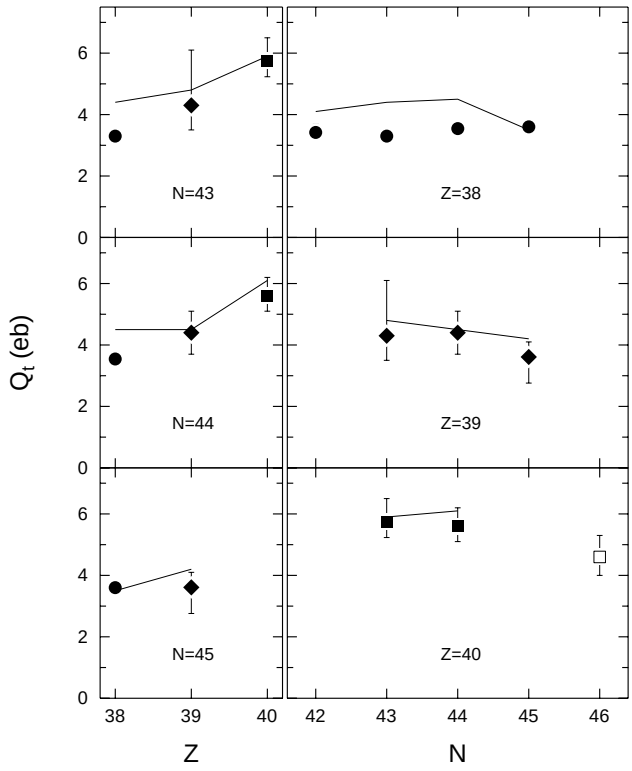

FIG. 11. Transition quadrupole moments measured for the yrast SD bands in $^{80-83}$Sr (circles), $^{82-84}$Y (diamonds), and ^{83,84,86}Zr (squares) as a function of Z (left) and N (right). The data point for ^{86}Zr (open symbol) is taken from Ref. [17]. The curves indicate the trend of the calculated Q_t values described in Sec. V C1.

B. Moments of inertia

The $\mathcal{J}^{(2)}$ moments of inertia for the SD bands extracted from the measured γ-ray energies are shown in Fig. 13. For all SD bands, the $\mathcal{J}^{(2)}$ values scatter around $25\hbar^2$/MeV, which is the typical value of the dynamic moment of inertia for the SD bands in this mass region. Most of the yrast SD bands exhibit a smooth behavior of $\mathcal{J}^{(2)}$ versus rotational frequency. Like in the mass-150 region of superdeformation, three different trends are observed—slightly upsloping, downsloping, and constant $\mathcal{J}^{(2)}(\omega)$ curves. The exceptions

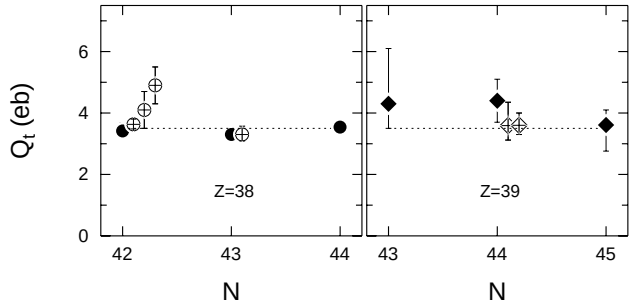

FIG. 12. Transition quadrupole moments measured for the excited SD bands in ^{80,81}Sr (left) and ^{83}Y (right) are compared with the Q_t values obtained for the yrast SD bands in the same nucleus and in neighboring isotopes. The values for the excited bands and the yrast bands are distinguished by open and filled symbols, respectively. The dotted line at 3.5 e b is to guide the eye.

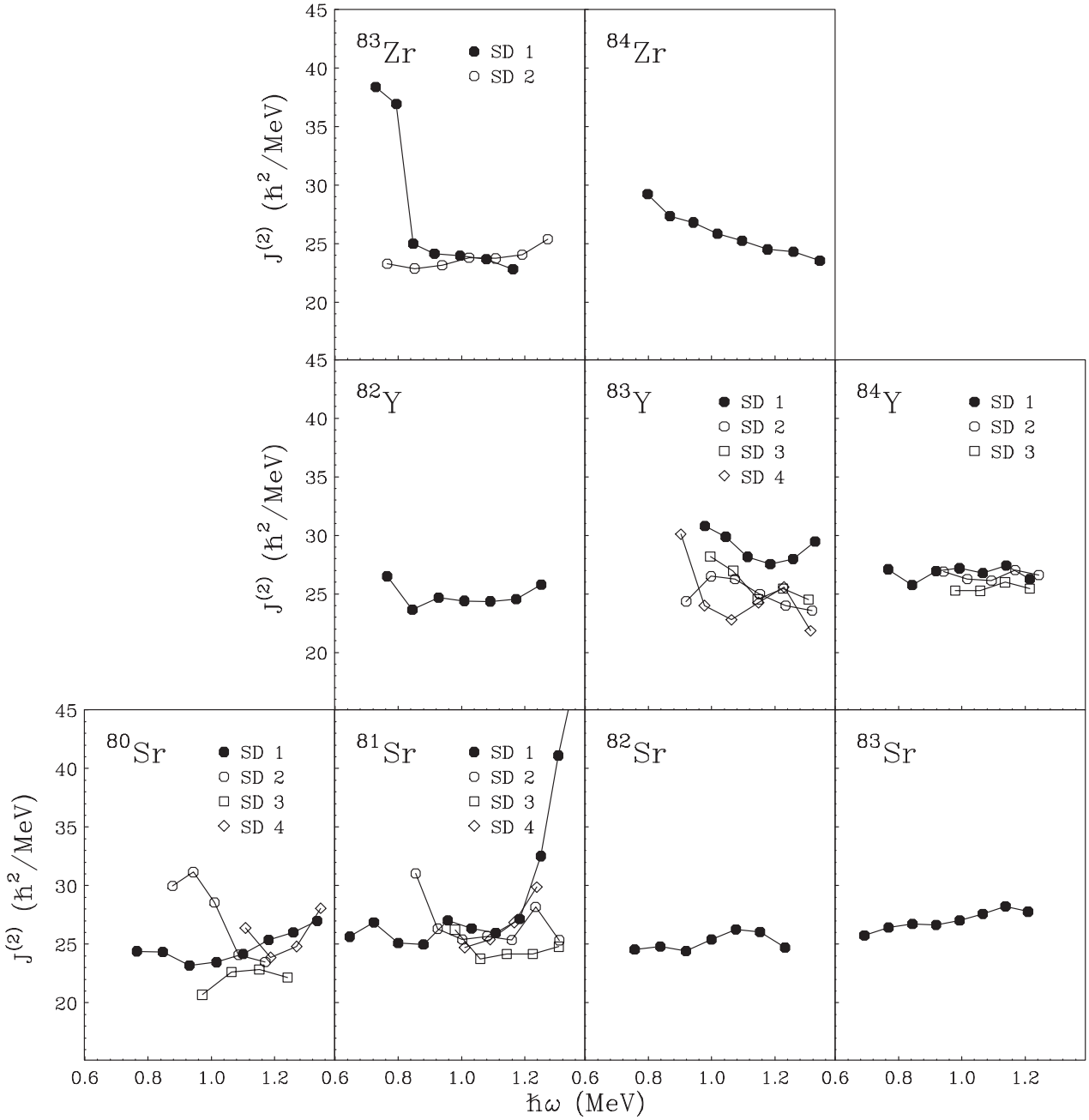

FIG. 13. Dynamical moments of inertia vs rotational frequency for all SD bands observed in this work. The yrast SD bands are represented by solid circles, first excited SD bands by open circles, second excited SD bands by open squares, and third excited SD bands by open diamonds. The lines connect the experimental points for clarity.

from a smooth $\mathcal{J}^{(2)}(\omega)$ behavior are (i) the yrast SD band in ^{83}Zr and a few excited SD bands in ^{80,81}Sr and ^{83}Y, with rising $\mathcal{J}^{(2)}$ values at low frequency, and (ii) the yrast SD bands in ^{81}Sr and ^{83}Y, which clearly show upbends at high frequency. In the case of ^{83}Zr, the low-frequency rise in $\mathcal{J}^{(2)}$ is likely due to a crossing with a less deformed structure, which is also indicated by the ''forking'' of states at the bottom of the yrast SD band [15]. The same explanation is probably true for the ''irregularities'' seen in ^{80,81}Sr and ^{83}Y. The upbends at high frequency for the yrast SD bands in ^{81}Sr and ^{83}Y, on the other hand, are attributed to a rotational alignment of a pair of nucleons. However, these upbends occur at different rotational frequencies, likely indicating that different pairs of nucleons are involved (see Sec. V C). It is interesting to recall that earlier, in Ref. [13], ''down-bending'' $\mathcal{J}^{(2)}$ values at high frequency were reported as a systematic feature of mass-80 SD bands. This statement is not supported by the present work (cf. Fig. 13).

Figure 13 indicates also that the band SD1 in ^{83}Y has a somewhat larger $\mathcal{J}^{(2)}$ moment than the yrast bands in the neighboring nuclei, e.g., the SD band in ^{84}Zr. However, the $\mathcal{J}^{(2)}$ moment of the yrast SD band in the $N=44$ isotone

TABLE IV. Proposed configuration assignments for the SD bands and calculated deformations, using the cranked Strutinsky approach. The values Q_t^{the} and the deformation parameters represent average values from the calculations for frequency ranges given in the last column. The assignments for the bands SD3 in ^{80}Sr and ^{83}Y are tentative. For ^{82}Y, two assignments are possible.

Structure	$Q_t^{\exp}$ (e b)	Config.	Q_t^{the} (e b)	$\beta_2^{the}, \gamma^{the}$	$\hbar\omega$[a]
^{80}Sr SD1	$3.42^{+0.26}_{-0.23}$	$\nu 5^1 \pi 5^0$	4.1	0.43, 2.6°	0.82–1.32
^{80}Sr SD2	$3.63^{+0.17}_{-0.15}$	$\nu 5^1 \pi 5^0$	4.3	0.44, 1.8°	0.81–1.22
^{80}Sr SD3	4.1 ± 0.6	$(\nu 5^1 \pi 5^0)$			
^{80}Sr SD4	4.9 ± 0.6	$\nu 5^1 \pi 5^1$	4.6	0.47, 9.0°	1.02–1.32
^{81}Sr SD1	$3.08^{+0.16}_{-0.15}$	$\nu 5^1 \pi 5^0$	4.4	0.46, 1.2°	0.61–1.31
^{81}Sr SD2	$3.30^{+0.27}_{-0.21}$	$\nu 5^1 \pi 5^0$	3.5	0.38, −8.3°	0.81–1.32
^{82}Sr	$3.54^{+0.15}_{-0.14}$	$\nu 5^1 \pi 5^0$	4.5	0.50, 6.0°	b
^{83}Sr	$3.60^{+0.20}_{-0.18}$	$\nu 5^1 \pi 5^0$	3.5	0.43, 13.0°	b
^{82}Y	$4.3^{+1.8}_{-0.8}$	$\nu 5^1 \pi 5^0$	4.8	0.47, 2.1°	0.72–1.23
		$\nu 5^1 \pi 5^1$	5.4	0.50, 4.3°	
^{83}Y SD1	4.4 ± 0.7	$\nu 5^1 \pi 5^1$	4.5	0.45, 9.9°	0.92–1.32
^{83}Y SD2	$3.6^{+0.8}_{-0.5}$	$\nu 5^1 \pi 5^0$			
^{83}Y SD3	$3.6^{+0.4}_{-0.3}$	$(\nu 5^0 \pi 5^0)$			
^{84}Y SD1	$3.6^{+0.5}_{-0.8}$	$\nu 5^1 \pi 5^0$	4.2	0.42, 11.1°	0.71–1.20
^{83}Zr	$5.8^{+0.8}_{-0.5}$	$\nu 5^2 \pi 5^1$	5.9	0.53, 4.6°	0.82–1.22
^{84}Zr	$5.6^{+0.6}_{-0.5}$	$\nu 5^2 \pi 5^1$	6.1	0.56, 3.5°	b

[a] Rotational-frequency ranges are given in MeV.
[b] Values of $\hbar\omega$, Q_t^{the}, and deformation parameters from Ref. [24].

^{85}Nb is of similar magnitude [18]. Hence, the $\mathcal{J}^{(2)}$moment for ^{83}Y does not happen to be an exception. The present attempts to describe this aspect of the data can be found in the following section.

C. Intruder orbital assignments

In order to clarify the underlying structure of the SD bands in $^{80-83}$Sr, ^{83}Y, and ^{84}Zr, their properties are compared with the results of theoretical calculations based on two different self-consistent mean-field methods. These are cranked Strutinsky Woods-Saxon calculations with pairing, using the Lipkin-Nogami approach (see, e.g., Refs. [33–35]), and cranked Hartree-Fock calculations without pairing [36,37]. Both theoretical approaches have shown that they provide an accurate description of rotational bands in different regions of superdeformation.

The final selection of the configuration that is assigned to a particular SD band is guided by the criterion that the calculated Q_t and $\mathcal{J}^{(2)}$ values should be close to the measured values. In addition, the excitation energy for the configuration under consideration relative to that of other relevant configurations is taken into account. The cranked Strutinsky approach is applied to all bands where a measured Q_t value is available, while Hartree-Fock calculations are presented only for a few cases and serve as a check. The results from both types of theoretical calculations are found to be consistent with each other. The configurations are described by the short-term notation $5^{\nu}5^{\pi}$with $\nu(\pi)$ being the number of $N_0 = 5$ neutron (proton) intruder orbitals occupied.

1. Description with the cranked Strutinsky approach

The calculations using the cranked Strutinsky approach lead to total Routhian surfaces (TRS). The total energy is minimized with respect to the shape parameters for the nuclear potential, β_2, β_4, and γ, and the rotational frequency and the lowest lying configuration is determined for a given parity and signature quantum number. As an extension to ''standard'' deformation self-consistent TRS calculations, the present model contains also pairing correlations, namely, of both the monopole and the quadrupole type. These are treated self-consistently by means of the Lipkin-Nogami method.

The $\mathcal{J}^{(2)}$ moment of inertia is calculated from the expectation value of the spin with respect to the rotational axis at a given frequency. The quadrupole moment as a function of rotational frequency is obtained from the expectation values for the Q_{20} operator.

Some of the Q_t values calculated with the cranked Strutinsky approach are presented in Fig. 11. From the comparison between the experiment and the calculations, it is obvious that the calculations reproduce the trends in the Q_t values for the yrast SD bands in $^{80-82}$Sr, ^{83}Y, and ^{84}Zr as a function of proton and neutron number. For the bands in the strontium nuclei, the calculations are higher by about 15% relative to the experiment. This discrepancy is likely due to a nonoptimal choice of the parameters for the potential (not optimal for the calculations of radial moments). However, most important for the configuration assignments are the consistent trends obtained in the experiment and the theory.

The configuration assignments based on the Q_t values and the $\mathcal{J}^{(2)}$ moments are summarized in Table IV. Notice that the theoretical Q_t values listed in the table represent the average values obtained for the range of rotational frequency observed in the experiment ($\hbar\omega \approx 1/2\, E_\gamma$). The $\mathcal{J}^{(2)}$ moments obtained from the cranked Strutinsky calculations are

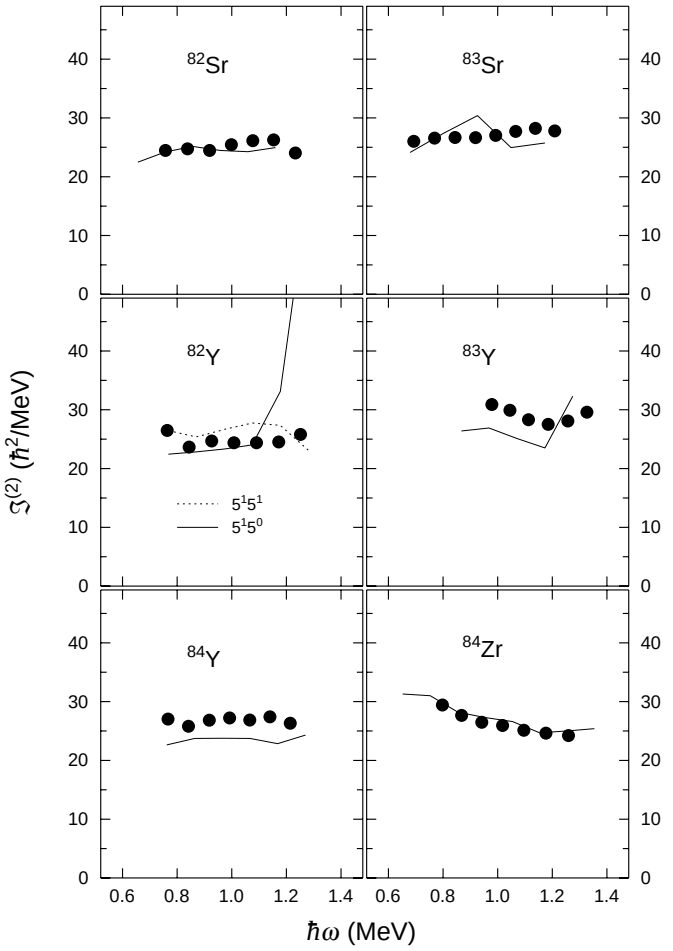

FIG. 14. The dynamical moments of inertia of the yrast SD bands in ^{82,83}Sr, $^{82-84}$Y, and ^{84}Zr as deduced from the experiment, in comparison with the values calculated with the cranked Strutinsky method. Measured values are shown in solid circles, calculated values are represented by lines. For ^{82}Y, two calculations are shown since the data do not favor a particular configuration.

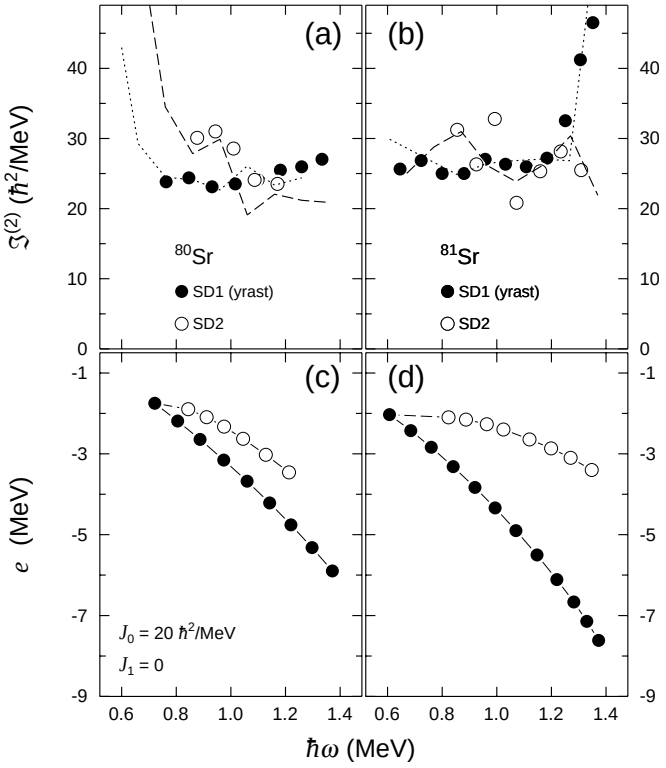

FIG. 15. Panels (a) and (b) give the $\mathcal{J}^{(2)}(\hbar\omega)$ moments of inertia for the two lowest SD bands in ^{80}Sr and ^{81}Sr, respectively, compared with the calculated values using the cranked Strutinsky method. Notice that the configuration for the yrast band in ^{81}Sr changes from 5^15^0 to 5^15^2 at $\hbar\omega\sim1.2$ MeV. Panels (c) and (d) give the Routhian energies $e'(\hbar\omega)$ for these bands in ^{80}Sr and ^{81}Sr, respectively, using the set of Harris parameters given in the figure. An assumption has been made about the excitation energies of these bands relative to each other at a fixed frequency (see text). The point of interest is the different splitting in e' with increasing $\hbar\omega$.

not included in the table but are discussed in the following paragraphs.

Figure 14 shows comparisons between the $\mathcal{J}^{(2)}$ moments calculated for the yrast SD bands in ^{82,83}Sr, $^{82-84}$Y, and ^{84}Zr by using the cranked Strutinsky approach and the corresponding values deduced from the experiment. The scatter for the calculated $\mathcal{J}^{(2)}$ moment for ^{83}Sr reflects some softness in the TRS maps for this nucleus with respect to the two deformation parameters β_2 and γ. Nevertheless, the $\mathcal{J}^{(2)}$ moment for this band as well as those for the yrast SD bands in the other strontium nuclei demonstrate good agreement between theory and experiment for the intruder orbital assignments proposed. Likewise, the properties of the SD bands in ^{84}Zr and ^{83}Zr can be reproduced by the calculations. For the bands in the yttrium nuclei, on the other hand, the level of agreement between experiment and theory is less satisfying. In the case of ^{82}Y, the assignment of a $\nu5^1\pi5^0$ or a $\nu5^1\pi5^1$configuration is possible, but due to the large experimental uncertainty for the Q_t value neither is favorable. The $\mathcal{J}^{(2)}$ moment calculated for the energetically lowerlying $\nu5^1\pi5^0$ configuration in this nucleus shows an upbend at $\sim$1.2 MeV that is not supported by the experiment and thus the assignment remains ambiguous. The already mentioned large $\mathcal{J}^{(2)}$ moment of the yrast SD band in ^{83}Y and the $\mathcal{J}^{(2)}$ moment for ^{84}Y cause a problem for the theory, which underpredicts this quantity for the configurations determined by the measured Q_t values (cf. Table IV).

In the top panels of Fig. 15, the $\mathcal{J}^{(2)}$ moments of the two lowest-lying SD bands in ^{80}Sr (left) and ^{81}Sr (right) are compared with the theoretical calculations. For both nuclei, the $\mathcal{J}^{(2)}$ moments of the yrast band and band SD2 are well described by the calculations for the $\nu5^1\pi5^0$ configuration, which has been chosen in accordance with the known Q_t values. For the yrast band in ^{81}Sr, a configuration change at the highest frequencies needs to be taken into account in order to describe the observed upbend. This upbend of $\mathcal{J}^{(2)}$ is attributed to the rotational alignment of a pair of protons in the $h_{11/2}$ intruder orbital, i.e., the top of the yrast SD band in ^{81}Sr represents a $\nu5^1\pi5^2$. This configuration change is associated with a significant deformation increase in the calculations. However, the $\langle\beta\rangle/\beta_0$ data are not sensitive to this effect.

The yrast SD bands and the SD2 bands in ^{80,81}Sr may be viewed as signature partner bands, based on the very similar Q_t values measured and a quite similar slope of their Routhian energies as a function of rotational frequency. The latter quantity, shown in the bottom panels of Fig. 15, is used to discuss further the $\nu 5^1\pi 5^0$ configuration assignment for these bands. For the purpose of comparing the energy splitting with increasing rotational frequency for the two sets of bands, the excitation energies of the bands relative to each other have been fixed at a certain low $\hbar\omega$ value. This assumption can be made and it does not affect the significant differences in the energy splitting seen between ^{80}Sr and ^{81}Sr. In the case of ^{81}Sr, it is a ''natural'' choice to view two lowest-lying bands as the two signatures of the $K=1/2$ $h_{11/2}$ intruder orbital[3] the odd neutron can occupy. This assignment is in accordance with the low energies calculated for these SD states. As a consequence, the signature splitting for this configuration is expected to be larger than that for other near-yrast configurations. In the case of ^{80}Sr, additional neutron states are involved in the excitation into the $h_{11/2}$ orbital (particle-hole excitations). Specifically, the Nilsson orbitals with $g_{9/2}$ (5/2[422]) and $d_{5/2}$ parentage (1/2[431]) are involved, according to calculations. The observed energy splitting should be the signature splitting for these configurations, since it is smaller than the splitting for the $h_{11/2}$ orbital. As shown in Fig. 15, the energy splitting with increasing frequency is indeed smaller for the SD bands in ^{80}Sr, which validates the configuration assignments made.

In the case of ^{80}Sr, Q_t values could be measured for all excited SD bands. For the two highest-lying (lowest intensity) bands, SD3 and SD4, large Q_t values (of $4.1^{+0.6}_{-0.6}$ and $4.9^{+0.6}_{-0.6}$ e b, respectively) were measured. The Q_t value for band SD4 requires a $\nu 5^1\pi 5^1$or $\nu 5^2\pi 5^0$ configuration assignment. The excitation of more intruder states than in the yrast configuration is consistent with the location of this band at a relatively high energy. For band SD3, a similar configuration or a $\nu 5^1\pi 5^0$ configuration is conceivable.

The results presented in Table IV lead to the following observations. The yrast SD bands in $^{80-83}$Sr and in ^{84}Y arise from $\nu 5^1\pi 5^0$ configurations, whereas the ^{83,84}Zr yrast SD bands and the ^{83}Y yrast SD band are assigned $\nu 5^2\pi 5^1$ and $\nu 5^1\pi 5^1$ configurations, respectively. In the case of the zirconium nuclei, another proton occupies the 1/2[431] Nilsson orbital. For these assignments, the SD bands in $^{80-83}$Sr are predicted to possess the smallest Q_t values, in agreement with the experiment. Similarly, most of the excited SD bands for which a Q_t value could be measured are described by the $\nu 5^1\pi 5^0$ excitation. The exception among the excited bands is the very excited band SD4 in ^{80}Sr, where a $\nu 5^1\pi 5^1$ or $\nu 5^2\pi 5^0$ configuration assignment is favored. Hence, for both the yrast and the excited SD bands a systematic correspondence between the number of $\nu h_{11/2}$ and $\pi h_{11/2}$ excitations and the measured Q_t values exists. As a consequence of these assignments, the isospectral SD bands are proposed to have the same intruder configuration ($\nu 5^1\pi 5^0$ for both sets of bands).

[3]The K quantum number represents the projection of the single-particle angular momentum on the symmetry axis of the nucleus and is used here to simplify the description.

TABLE V. Proposed configuration assignments for some mass-80 SD bands from the Hartree-Fock calculations. The values Q_t^{the} represent average values for the frequency ranges in the calculations that overlap with the experimental observations.

Structure	$Q_t^{\exp}$ (e b)	Configuration	Q_t^{the} (e b)
^{82}Sr	$3.54^{+0.15}_{-0.14}$	$\nu 5^1\pi 5^0$	3.9
^{83}Sr	$3.60^{+0.20}_{-0.18}$	$\nu 5^1\pi 5^0$	3.8
^{82}Y	$4.3^{+1.8}_{-0.8}$	$\nu 5^1\pi 5^0$	4.8
^{83}Y SD1	$4.4^{+0.7}_{-0.7}$	$\nu 5^1\pi 5^1$	4.3
^{83}Y SD2	$3.6^{+0.8}_{-0.5}$	$\nu 5^1\pi 5^0$	4.1
^{83}Y SD3	$3.6^{+0.4}_{-0.3}$	$\nu 5^0\pi 5^0$	3.8

2. Description with the Hartree-Fock approach

The properties of some of the SD bands under discussion are also compared with results from cranked Hartree-Fock calculations. The Hartree-Fock calculations have been carried out using the Skyrme SLy4 [38] effective interaction and no pairing (see Ref. [36,37] for details). Like in the preceding section, the configuration assignments are guided mainly by the Q_t and $\mathcal{J}^{(2)}$ moments. The results from the Hartree-Fock calculations are summarized in Table V.

The quadrupole moments calculated for the SD structures listed in Table V are consistent with the results from the cranked Strutinsky calculations. However, for the SD band in ^{82}Y a $\nu 5^1\pi 5^0$ configuration assignment is favored by the Hartree-Fock calculations. The level of agreement between the calculated $\mathcal{J}^{(2)}$ moment for this energetically lowest-lying intruder configuration and the measured $\mathcal{J}^{(2)}$ value is documented in Fig. 16. The high-frequency upbend obtained for the calculated $\mathcal{J}^{(2)}$ values (above 1.3 MeV) is due to a crossing of the $\nu 5^1\pi 5^0$ configuration with the $\nu 5^1\pi 5^1$ or $\nu 5^2\pi 5^0$ configuration but there is no inconsistency with the experimental values. This removes the ambiquity in Fig. 14 and Table IV. For the $\nu 5^1\pi 5^0$ configuration in ^{82}Y, a larger Q_t^{the} value is calculated than for the $\nu 5^1\pi 5^1$ configuration in ^{83}Y (cf. Table IV). This difference is, in part, due to a larger occupation probability for the 3/2[301] neutron orbital, when going from ^{82}Y to ^{83}Y, which tends to reduce the deformation.

Figure 17 illustrates the comparisons between experimentally observed and calculated quantities for the yrast and excited SD bands in ^{83}Y. In the left panels, the quadrupole moments are presented as a function of rotational frequency, where the box represents the average Q_t value with uncertainty and the range of γ-ray energies ($E_\gamma \approx 2\hbar\omega$) in which the $\langle\beta\rangle/\beta_0$ measurement is performed (cf. Fig. 9).

For the yrast SD band in ^{83}Y, the measured Q_t value is best described by the $\nu 5^1\pi 5^1$ configuration (dotted curve),

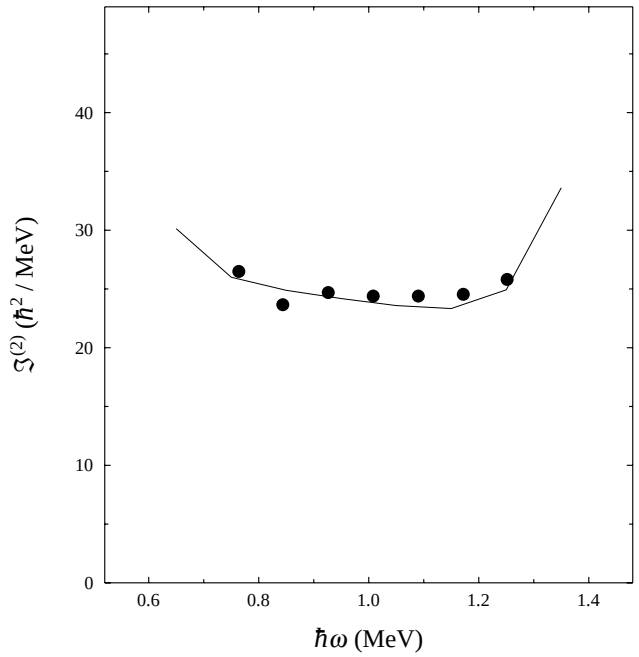

FIG. 16. The dynamical moment of inertia for the SD band in ^{82}Y in comparison with the calculated value for the $\nu 5^1 \pi 5^0$ configuration, using the cranked Hartree-Fock method.

while the alternatively considered $\nu 5^2 \pi 5^1$ configuration (dashed) overpredicts this quantity. The $\mathcal{J}^{(2)}$ moment, on the other hand, does not favor either of these two configurations. Specifically, the Hartree-Fock calculations underpredict the

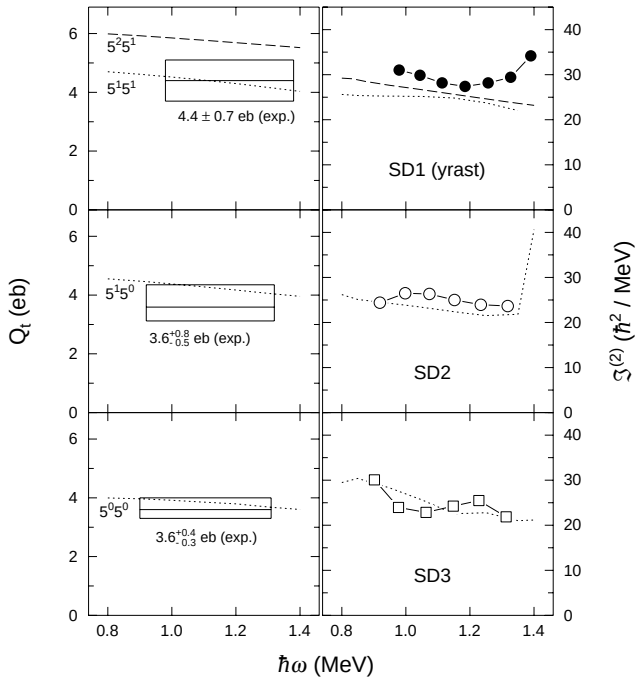

FIG. 17. The Q_t values (left) and the $\mathcal{J}^{(2)}$ moments (right) of the SD bands in ^{83}Y compared with the results from the Hartree-Fock calculations. The properties of the yrast band and the excited bands, SD2 and SD3, are presented in the top, middle, and bottom panels, respectively.

$\mathcal{J}^{(2)}$ moment of the yrast SD band in ^{83}Y like the cranked Strutinsky calculations do. For the ^{83}Y excited SD bands, the Q_t values of 3.6 *e* b are remarkably well reproduced by the $\nu 5^1 \pi 5^0$ and $\nu 5^0 \pi 5^0$ configurations. The latter one should be qualified as a highly deformed configuration. As shown in the right panels (middle and bottom), the $\mathcal{J}^{(2)}$ moments of the excited SD bands in ^{83}Y are fairly well reproduced by the Hartree-Fock calculations for the $\nu 5^1 \pi 5^0$ and $\nu 5^0 \pi 5^0$ configurations. Overall, the assignments in Table V are reasonably well justified.

3. Concluding remarks

The results in the present paper and in Ref. [24] lead to some revisions of previous intruder orbital assignments. The proposed configuration changes affect mainly the yrast and excited SD bands in the strontium isotopes that have been discussed previously in Refs. [9,10,13]. These earlier assignments predicted a moderate increase of the Q_t values of the yrast SD bands across the isotopes $^{80-83}$Sr. The present experimental results, on the other hand, indicate rather constant Q_t values for the $^{80-83}$Sr cases, including their lowest-lying excited bands. One of the conclusions from the present work is that there are distinctly fewer $h_{11/2}$ excitations necessary to describe the configurations of the yrast SD bands in ^{82,83}Sr than the authors of Refs. [7,8,11,12] assumed. This difference may be understood as follows.

In the cranked Strutinsky calculations, the $N=Z=38$ energy gap at highly deformed shapes ($\beta_2 \gtrsim 0.4$) is stable up to the highest frequencies experimentally observed. Hence, the promotion of protons into the intruder orbitals from the $N_0=5$ shell is, for the strontium isotopes, not energetically favorable. The present Q_t measurements confirm the expected stability of the $Z=38$ gap, which, however, prevents the secondary minimum of a strontium nucleus from assuming the same SD shape as, e.g., ^{84}Zr. Hence, only the neutron configuration in $^{80-83}$Sr is characterized by the occupation of an $N_0=5$ intruder orbital, but only a single one. Therefore, the bands in $^{80-83}$Sr (and perhaps also an excited band in ^{83}Y) may be qualified as highly deformed prolate rotors ($\beta_2 \lesssim 0.5$).

In this context, it is interesting to notice that band SD3 in ^{81}Sr, which interacts with the yrast SD band, does not resemble any low-lying configuration that would involve an excitation into the $N_0=5$ shell and match the parity and spin of the yrast band. Instead, all candidate configurations are located too high in energy. Therefore, band SD3 could be a normal or highly deformed structure located at a similar excitation energy as the neutron $h_{11/2}$ intruder bands in ^{81}Sr. This scenario is also consistent with another fact: The interaction strength obtained for the cross-talk between SD1 and SD3 ($V_{int} \approx 6$ keV) is rather small when compared with reported cases of crossings between SD states, viz., in ^{87}Nb [19] (two interactions with $V_{int} \approx 47$ and 70 keV). This seems to support the picture of an accidental interaction, in contrast to those ''expected'' crossings.

A general theme in the present and in previous work on mass-80 SD states is the SD shell gap for the proton system. Notably, in ^{81}Sr the upbend in the $\mathcal{J}^{(2)}$ values for the yrast

TABLE VI. Orbitals other than intruders discussed for mass-80 SD bands. When two orbitals are listed the configuration is mixed.

Structure	Nonintruder orbitals	Comment
^{80}Sr SD1	$\nu g_{9/2}(5/2[422])$, $\nu d_{5/2}(1/2[431])$	Signature partner
^{80}Sr SD2	$\nu g_{9/2}(5/2[422])$, $\nu d_{5/2}(1/2[431])$	Signature partner
^{82}Sr SD	$\pi f_{5/2}, p_{3/2}(1/2[310])$	Isospectral
^{83}Sr SD	$\pi f_{5/2}, p_{3/2}(1/2[310])$	Isospectral
^{83}Y SD1	$\nu f_{5/2}, p_{3/2}(3/2[301)]$	
^{83}Y SD2	$\pi f_{5/2}, p_{3/2}(1/2[310])$	Isospectral
^{84}Y SD1	$\pi f_{5/2}, p_{3/2}(1/2[310])$	Isospectral
^{83}Zr SD1	$\pi d_{5/2}(1/2[431])$	
^{84}Zr SD	$\pi d_{5/2}(1/2[431])$	

SD band reflects the occupation of the proton $h_{11/2}$ intruder orbital at high frequency leading to a rearrangement of the second well vacuum configuration. There is also a difference in the structure of the bands in the second well between proton numbers $Z=38$ and $Z=40$. Indeed, as shown in Fig. 11, the Q_t values increase from $Z=38$ to $Z=40$ with the yttrium nuclei showing a ''transitional'' behavior with respect to this deformation change. By the same token, a proton $h_{11/2}$ excitation is not only energetically accessible but stabilizes the equilibrium deformation for the SD shape.

For the neutron system, a ''magic'' SD gap at $\beta_2 \approx 0.6$ is obtained for $N=44$. Unlike the $Z=40$ gap, this neutron gap is stable over a large frequency range. It leads to the occupation of a pair of $h_{11/2}$ neutrons in ^{84}Zr and ^{83}Zr, the two nuclei with the largest quadrupole deformation observed in the present work. The band in ^{84}Zr is (together with the yrast SD band in ^{83}Zr) also the most strongly populated SD band under discussion. Hence, it is reasonable to view ^{84}Zr as the doubly magic nucleus in the mass-80 region of superdeformation.

For $N=43$, but at a somewhat smaller deformation $\beta_2 < 0.6$, a rather pronounced energy gap for the neutron orbitals occurs as well. However, the earlier expectation that when passing from $N=43$ to $N=44$ the quadrupole moment may increase (by $\sim 0.6\ e$ b) is not supported by the present work. On the other hand, the $N=44$ gap seems to stabilize the SD shape against deviations from axial symmetry. Values for the deformation parameter γ that deviate considerably from 0 (by more than 10°) are calculated for the $N=45$ systems, ^{83}Sr and ^{84}Y (Table IV), and the $N=46$ system, ^{86}Zr [17]. This prediction seems to be in line with the Q_t values measured for these three nuclei, which are somewhat smaller than those for their lighter isotopes (cf. Fig. 11).

Finally, a comment about the features of the two pairs of isospectral SD bands studied in the present work: Like most of the isospectral bands in the mass-150 and mass-190 regions of superdeformation, these pairs of SD bands possess very similar Q_t values, which seems to be characteristic for the isospectral band phenomenon. The similar Q_t values for the ^{82} Sr, ^{83}Y (SD2) pair and for the ^{83}Sr, ^{84}Y (SD1) pair are attributed to a common $\nu 5^1 \pi 5^0$ configuration in both cases. The question is then, how to describe the very similar $\mathcal{J}^{(2)}$ moments of inertia, which are in both cases ''flat'' throughout the entire frequency range. The best candidate for an orbital causing this behavior is the proton $f_{5/2}-p_{3/2}$ (1/2[310]) orbital, which approaches the Fermi surface for $Z=39$ at a deformation $\beta_2 \gtrsim 0.4$. In the frequency range of interest, it is essentially constant and, thus, the alignment and $\mathcal{J}^{(2)}$ contributions from this orbital are nearly zero. In this picture, the 1/2[310] orbital would be occupied by the 39th proton in the yttrium nuclei. Removing the 39th proton from this orbital would then result in a configuration for the strontium nuclei with very similar $\mathcal{J}^{(2)}$ moments. This orbital and the other ''normal'' orbitals in the $f-p-g$ shell and the $d_{5/2}$ shell that have been discussed in the present paper are also listed for clarity in Table VI.

VI. SUMMARY

Results of an experiment are presented in which the average transition quadrupole moments for most of the SD bands in the nuclei $^{80-83}$Sr, $^{82-84}$Y, and ^{83,84}Zr have been measured accurately and under nearly identical experimental conditions. These results include also measurements for several excited SD bands. The Q_t values together with the dynamical moments of inertia established from the experiment allow one to make stringent comparisons with deformation and pairing self-consistent mean-field calculations. From these comparisons, reliable configuration assignments for the SD bands are obtained. Notably, some of the yrast and the first excited SD bands can be viewed as signature partner bands.

The ''magic'' configuration ($\nu 5^2 \pi 5^1$) is represented best by the SD band in ^{84}Zr. The presence of SD shell gaps at $Z=40$, $N=44$, as predicted by the theoretical calculations, is supported by the present data. The $Z=40$ gap occurs only for a considerable rotation of the system (in the frequency range the SD bands are observed). Therefore, the SD bands around ^{84}Zr are rather outstanding examples for shape stabilization by rotational frequency or angular momentum.

Another point of interest are the Q_t values measured for the two pairs of isospectral bands present in the data, which are found to be nearly identical. These are the first two examples for isospectral SD bands below the mass-150 and

mass-190 regions of superdeformation and there are common characteristics established for these bands in all three regions.

The present experiment represents the highest statistics dataset for the mass 80 region reported so far. However, no linking transitions between the SD and normal states nor $M1$ signature partner linking transitions between the SD bands have been observed yet in any nucleus in this region.

ACKNOWLEDGMENTS

This work was supported in part by the U.S. Department of Energy under Grant No. DE-FG02-88ER-40406, the U.S. DOE Contract Nos. DE-AC05-00OR2222725 and DE-AC03-76SF00098, the U.S. NSF Grant No. PHY-9523974, by the Swedish Natural Science Research Council, and by the Polish Committee for Scientific Research (KBN).

[1] W. Nazarewicz, J. Dudek, R. Bengtsson, T. Bengtsson, and I. Ragnarsson, Nucl. Phys. **A435**, 397 (1985).
[2] J. Dudek, W. Nazarewicz, and N. Rowley, Phys. Rev. C **35**, 1489 (1987).
[3] T. Bengtsson, I. Ragnarsson, and S. Åberg, Phys. Lett. B **208**, 39 (1988).
[4] P. Bonche, H. Flocard, and P.H. Heenen, Nucl. Phys. **A523**, 300 (1991).
[5] T. Werner and J. Dudek, At. Data Nucl. Data Tables **50**, 176 (1992).
[6] A.V. Afanasjev and I. Ragnarsson, Nucl. Phys. **A586**, 377 (1995).
[7] C. Baktash, D.M. Cullen, J.D. Garrett, C.J. Gross, N.R. Johnson, W. Nazarewicz, D.G. Sarantites, J. Simpson, and T.R. Werner, Phys. Rev. Lett. **74**, 1946 (1995).
[8] D.R. LaFosse *et al.*, Phys. Lett. B **354**, 34 (1995).
[9] M. Devlin *et al.*, Phys. Lett. B **415**, 328 (1997).
[10] F. Cristancho *et al.*, Phys. Lett. B **357**, 281 (1995).
[11] C.H. Yu *et al.*, Phys. Rev. C **57**, 113 (1998).
[12] A.G. Smith *et al.*, Phys. Lett. B **355**, 32 (1995).
[13] P.J. Dagnall *et al.*, Z. Phys. A **353**, 251 (1995).
[14] H.-Q. Jin *et al.*, Report No. ANL-PHY-96/1, 1996 (unpublished).
[15] D. Rudolph *et al.*, Phys. Lett. B **389**, 463 (1996).
[16] H.-Q. Jin *et al.*, Phys. Rev. Lett. **75**, 1471 (1995).
[17] D.G. Sarantites *et al.*, Phys. Rev. C **57**, R1 (1998).
[18] D. R. LaFosse *et al.* (unpublished).
[19] D.R. LaFosse *et al.*, Phys. Rev. Lett. **78**, 614 (1997).
[20] T. Bäck *et al.*, Eur. Phys. J. A **6**, 391 (1999).
[21] B. Cederwall *et al.*, Eur. Phys. J. A **6**, 251 (1999).
[22] E. Ideguchi *et al.*, Phys. Lett. B **492**, 245 (2000).
[23] B. Cederwall *et al.*, Nucl. Instrum. Methods Phys. Res. A **354**, 591 (1995).
[24] F. Lerma *et al.*, Phys. Rev. Lett. **83**, 5447 (1999).
[25] I. Lee, Nucl. Phys. **A520**, 641c (1990).
[26] D.G. Sarantites, P.F. Hua, M. Devlin, L.G. Sobotka, J. Elson, J.T. Hood, D.R. LaFosse, and J.E. Sarantites, Nucl. Instrum. Methods Phys. Res. A **381**, 418 (1996).
[27] M. Devlin, L.G. Sobotka, D.G. Sarantites, and D.R. LaFosse, Nucl. Instrum. Methods Phys. Res. A **383**, 506 (1996).
[28] C.E. Svensson *et al.*, Nucl. Instrum. Methods Phys. Res. A **396**, 228 (1996).
[29] J.A. Becker *et al.*, Phys. Rev. C **46**, 889 (1992), and references therein.
[30] I. Lee (private communication).
[31] J. F. Ziegler, J. P. Biersack, and U. Littmark, *The Stopping and Ranges of Ions in Matter* (Pergamon, London, 1985), Vol. 1.
[32] C.-H. Yu (private communication).
[33] W. Satuła and R. Wyss, Phys. Scr. **T56**, 159 (1995).
[34] W. Satuła and R. Wyss, Phys. Rev. C **50**, 2888 (1994).
[35] R. Wyss and W. Satula, Phys. Lett. B **351**, 393 (1995).
[36] J. Dobaczewski and J. Dudek, Comput. Phys. Commun. **102**, 166 (1997).
[37] J. Dobaczewski and J. Dudek, Comput. Phys. Commun. **131**, 164 (2000).
[38] E. Chabanat, P. Bonche, P. Haensel, J. Meyer, and F. Schaeffer, Nucl. Phys. **A635**, 231 (1998).